# Distributed Dynamic Event-Triggered Control for Voltage Recovery in Islanded Microgrids by Using Artificial Delays

Amedeo Andreotti, Bianca Caiazzo, *Member, IEEE*, Emilia Fridman, *Fellow, IEEE*, Alberto Petrillo, *Member, IEEE*, and Stefania Santini, *Member, IEEE*

***Abstract*—This article tackles secondary voltage recovery problem in islanded microgrids with the aim of reducing communication frequency among distributed generation (DG) units, while maintaining desired performance and saving communication network workload. To pursue this objective, a distributed proportional-integral-derivative controller is first introduced, whose sampled-data implementation is enabled by leveraging the finite-difference approximation for the derivative action, which leads to a distributed proportional-integral-retarded (PIR) controller with a small enough sampling period $h > 0$. Then, the resulting fully distributed PIR control law is combined with a dynamic event-triggered mechanism (DETM), which embeds Zeno-freeness property and avoids the requirement of continuous transmission in triggering process. Thus, the communication burden is significantly mitigated and the waste of communication resources is avoided. By exploiting Lyapunov–Krasovkii method, we derive exponential stability conditions expressed as linear matrix inequalities (LMIs), whose solution allows evaluating the maximum sampling period and DETM parameters preserving the stability of the microgrid. A thorough numerical analysis, carried out on the standard IEEE 14-bus test system, confirms the theoretical derivation.**

***Index Terms*—Artificial delays, dynamic event-triggered control (ETC), IEEE 14-bus test system, islanded microgrid, Lyapunov–Krasovkii (LK) method, secondary voltage control.**

## I. Introduction

DRIVEN by the desire of moving to a low-carbon energy future, the next generation of power systems, referred as smart grids (SGs), is approaching, where monitoring, communication, coordination and control become key tasks for a more efficient use of energy [1]. As elementary units of SGs, microgrids (MGs) integrate renewable distributed generation (DG) units and energy storage systems (ESSs), able to supply local loads in small geographic areas, while mitigating environmental concerns [2]. The combination of these physical plants with measurements and control loops let the MGs to be investigated as cyber–physical systems (CPSs). Thanks to its capability to connect/disconnect from the utility grid, a MG can operate in either grid-connected or islanded modes. In islanded mode, the MG works autonomously and possible mismatches between the generated power and loads may result in voltage/frequency instability. Therefore, the control loops over a communication networks are fundamental in this operational mode.

Since several requirements with different time scales have to be guaranteed, a three-layers hierarchical control architecture is commonly exploited for MG control [3]. The primary control (PC) layer is usually based on droop-control, which is a communication-free method. While the tertiary control (TC) deals with economic aspects, the secondary control (SC) is required to adjust unavoidable frequency/voltage deviations induced by the PC. The focus of this manuscript is the voltage regulation problem which, falling into SC layer, is the more critical level to guarantee nominal working conditions. At this level, distributed control schemes are gaining momentum since they represent a superior alternative in terms of flexibility, reliability and scalability w.r.t. conventional centralized or decentralized approaches. Along this line, cooperative control of multiagent systems (MASs) represents one of the main approaches for SC design [4]. Several distributed control strategies are introduced for the voltage regulation problem in MGs, each of them facing a specific challenge, such as finite-time convergence [3], [5], bounded uncertainties/disturbances [6], and cyber-attacks [7], [8], [9]. For instance, false data injection (FDI) attacks are considered in [8], where a distributed observer is introduced to obtain an accurate estimation of the attack signals, while a resilient controller is exploited for attacks compensation. The simultaneous presence of communication delays and Denial-of-Service (DoS) attacks is counteracted in [9] via a novel time-varying sampling scheme with an improved communication mechanism, thus enhancing the resilience of the MG.

All the aforementioned solutions assume continuous communication among DGs and require fast communication ability to ensure the stability of the system, which may lead to heavy burden on the communication network, especially when the number of DGs increases [10]. Therefore, the design

Manuscript received 8 May 2023; revised 14 August 2023, 13 November 2023, and 22 January 2024; accepted 7 February 2024. This article was recommended by Associate Editor Y. Tan. *(Corresponding author: Bianca Caiazzo.)*

Amedeo Andreotti, Bianca Caiazzo, Alberto Petrillo, and Stefania Santini are with the Department of Electrical Engineering and Information Technology, University of Napoli Federico II, 80125 Naples, Italy (e-mail: amedeo.andreotti@unina.it; bianca.caiazzo@unina.it; alberto.petrillo@unina.it; stefania.santini@unina.it).

Emilia Fridman is with the School of Electrical Engineering, Tel Aviv University, Tel Aviv 69978, Israel (e-mail: emilia@tauex.tau.ac.il).

Color versions of one or more figures in this article are available at https://doi.org/10.1109/TCYB.2024.3364820.

Digital Object Identifier 10.1109/TCYB.2024.3364820

of effective and reliable control schemes for the resulting networked control system (NCS), able to reduce the data exchange frequency, will be meaningful in order to: 1) efficiently manage the limited bandwidth; 2) reduce network congestion; and 3) avoid waste of communication and computation resources, including workload between controllers and the related actuators [10], [11]. Event-triggered control (ETC) has been recognized as a suitable solution to achieve the aforementioned objectives and avoid costly communication, as well as higher workload [12], [13].

Along this direction, distributed ETC is proposed to achieve SC objectives in [11], where the design of triggering function has been handled via Lyapunov method. An ETC has been embedded into a distributed model predictive control (DMPC) scheme in [14] to regulate the voltage magnitude of each DG, where it is shown that communication/computation burden is reduced with slightly compromised control performance. Herein, to improve these latter, authors also embed an adaptive observer to mitigate the negative effects of mismatches due to sampling process. The presence of communication time-delays during information sharing process has been considered in [15], where the voltage synchronization is achieved via a distributed ETC through the low-gain feedback technique. Note that, all the above-mentioned ETC methods are designed without considering disturbances acting on DG dynamics and, hence, they may not guarantee Zeno-freeness in practical applications [10].

From this literature overview, it is clear that most efforts have been done toward the development of static ET rules based on synchronization/sampling voltage errors [16]. However, dynamic ET mechanism (DETM), based on an auxiliary internal variable, is gaining attention in the last years since it has been proven to require fewer control updates w.r.t. static ET control and to eliminate Zeno behavior [17], [18]. The main difference between static ET and the dynamic one relies in the threshold. Static ET has a fixed and constant threshold into the triggering rule, whereas DET endows a dynamically adjustable mechanism, provided by the additional internal variable [19]. Therefore, due to the several merits of DET control, including significantly larger average interevent time, several DET-based control strategies have been introduced in the context of consensus control problem of MASs (see, e.g., [20], [21], and [22]). Along this direction, DET-based controller is proposed for MG voltage SC in [19], where the triggering mechanism, dependent on the voltage error measurements, is applied along with a simple fully diffusive control protocol. However, the unavoidable external disturbances are not considered and, hence, Zeno behavior could not be avoided.

In light of the above, the aim of this work is to propose a novel *communication resources saving-oriented* control architecture which embeds a robust distributed DET proportional-integral-derivative (PID)-like controller able to solve voltage recovery problem in inverter-based islanded MG. Bounded disturbances, arising from MG modeling phase, are taken into account without compromise Zeno-freeness property. Hence, the control design objective is two-fold, namely, 1) to propose a distributed MG voltage control scheme which does not require continuous interagent interactions, no longer valid in distributed control over communication networks [23] and 2) to provide a novel dynamic triggering rule to further reduce the number of actuator updates and, hence, the amounts of communication network workload from controller-to-actuator. The combination of 1) and 2) allows saving all the communication resources involved into the MG control architecture from NCS perspective. By exploiting artificial delay technique (i.e., intentionally introduced delay as explained in Remark 2 below) and finite-difference approximation [24], the first objective is achieved by recasting the fully distributed PID-like control protocol in a sampled-data proportional-integral-retarded (PIR) controller so to obtain a preliminary reduction of the communication network workload. On the other hand, the novel proposed DETM is able to further reduce the number of the control signals sent to actuators according to control objective *ii*). This is achieved via the additional internal variable which adjusts the triggering threshold and lengthens the interevent time intervals. Moreover, it is worth noting that our DETM is based on control signals, instead of voltage errors measurements, in order to avoid accumulating errors in the integral terms approximation.

The data sampling is tackled via time-delay approach, which is based on Lyapunov–Krasovkii (LK) method and Wirtinger's inequality [25], where the key point is to express the delayed term via its Taylor's expansion with remainder in the integral form, properly compensated via the LK functional. Thus, simple robust sampling-dependent stability conditions in the form of linear matrix inequalities (LMIs) are derived, whose feasibility is ensured for small enough sampling period if the original distributed derivative-dependent controller stabilizes the MG voltage.

Summarizing, the main contributions of this article are as follows.

1) The exploitation of artificial delays technique allows deriving a sampled-data distributed controller which, underlying the proposed DETM, ensures that continuous information exchanges among DGs are always avoided and its real implementation in digital control platform becomes easier; thus, the actual challenge in distributed control of MASs of re-evaluating conventional distributed continuous-time controllers in a sampled-data fashion is addressed [23].
2) Unlike [2], [26], [27], [28], the proposed DETM is fully distributed, that is, it is independent of any global information, such as the eigenvalues of the matrices, associated with the communication topology.
3) Compared with static ETC [11], [26], [27], our triggering mechanism is dynamic with an auxiliary internal variable reducing the interevent times and including conventional static ETC as a special case.
4) Differently from the very recent DETM strategies proposed in [19], which neglects the presence of disturbances, our stability analysis allows tuning the DETM parameters as a solution of a feasible LMIs problem.
5) Compared with the conference version of this article [29], herein we further reduce the usage of the limited communication resources with a less number of

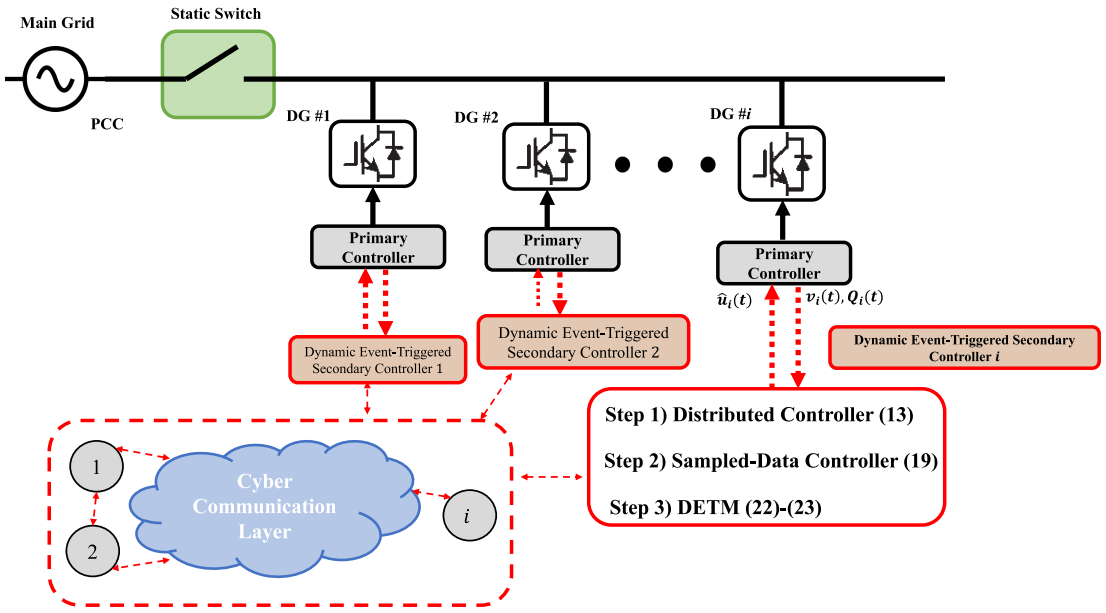


Fig. 1. Distributed dynamic event-trigger PID control architecture for SC voltage regulation.

triggering events, which is helpful for saving communication bandwidth from controller-to-actuator.

Finally, this article structure is as follows. In Section II the cyber–physical model of an islanded MG is introduced. The proposed distributed secondary DET PIR voltage controller is designed in detail in Section III. Section IV provides the stability analysis based on LK method. Finally, extensive numerical results are presented in Section V, while conclusions are drawn in Section VI.

*Notation:* Throughout this article, $\mathbb{N}_0 = \mathbb{N} \cup \{0\}$, the superscript $\top$ stands for matrix transposition, $\mathbb{R}^n$ denotes the $n$ dimensional Euclidean space, $\mathbb{R}^{n\times m}$ is the set of all $n \times m$ real matrices. The notation $P > 0$, for $P \in \mathbb{R}^{n\times n}$, means that $P$ is symmetric and positive definite. The symmetric elements of the symmetric matrix are denoted by $\star$. $I_N$ is the identity $n \times n$ matrix, $\otimes$ represents the Kronecker product and $\text{diag}\{a_i\}_{i=1}^n$ stands for a diagonal matrix with $a_i$ being on the diagonal.

*Lemma 1 (Exponential Wirtinger's Inequality [24], [25]):* Let $f : [a, b] \to \mathbb{R}^n$ be an absolutely continuous function with a square integrable first order derivative such that $f(a) = 0$ or $f(b) = 0$. Then, for any $\alpha \in \mathbb{R}$ and $0 \leq W \in \mathbb{R}^{n\times n}$

$$\int_a^b e^{2\alpha t} f^\top(t) W f(t)\, dt \leq e^{2|\alpha|(b-a)} \frac{4(b-a)^2}{\pi^2} \times \int_a^b e^{2\alpha t} \dot{f}^\top(t) W \dot{f}(t)\, dt.$$

*Lemma 2 (Jensen's Inequality [24]):* Let $\rho : [a, b] \to [0, \infty)$ and $f : [a, b] \to \mathbb{R}^n$ be such that the integration concerned is well-defined. Then, for any $0 < Q \in \mathbb{R}^{n\times n}$

$$\left[\int_b^b \rho(s) f(s)\, ds\right]^\top Q \left[\int_b^b \rho(s) f(s)\, ds\right] \leq \int_a^b \rho(s)\, ds \int_a^b \rho(s) f^\top(s) Q f(s)\, ds.$$

## II. Primary and Secondary Control of Microgrids

Consider an islanded AC MG involving $N$ DGs and $M$ loads. As depicted in Fig. 1, a PC layer is involved in the generic $i$th DG, which stabilizes the MG and guarantees the power sharing capability [30]. The $i$th DG PC consists of power, voltage and current inner control loops, where the time separation operation is required due to their different time scales. Voltage and current control loops usually follow the traditional PI controllers (see [31] and references therein).

Although the PC of each DG is generally formulated under its own $d-q$ (direct-quadrature) reference frame rotating at the frequency $\omega_i$, all the DGs choose a common reference frame to operate with the rotating frequency $\omega_{\text{com}}$. Denote the angle of the $i$th DG reference frame with respect to the common reference frame as

$$\delta_i = \int (\omega_i - \omega_{\text{com}})\, dt. \tag{1}$$

In $d-q$ synchronous frame with $d$-axis voltage aligning with the MG bus terminal voltage, the $i$th DG can be represented via the following droop-based equations:

$$\begin{cases} \begin{cases} k_{v_i} \dot{v}_i^{od} = v_i^n - v_i^{od} - n_i^Q Q_i^m \\ v_i^{oq} = 0 \end{cases} \\ \omega_i = \omega_i^n - m_i^P P_i^m \end{cases} \tag{2}$$

where $v_i^{od}$ and $v_i^{oq}$ are the voltage $d-q$ components of the $i$th DG; $v_i^n$ and $\omega_i^n$, provided by the SC layer, represent the PC voltage and frequency set-points; $P_i^m$ and $Q_i^m$ are the measured active and reactive power at the $i$th DG terminal; $k_{v_i} \in \mathbb{R}^+$ is the voltage control gain; and $n_i^Q \in \mathbb{R}^+$ and $m_i^P \in \mathbb{R}^+$ are its voltage and frequency droop coefficients, respectively. $P_i^m$ and $Q_i^m$ are provided by first-order low-pass filter [32]

$$\tau_{P_i} \dot{P}_i^m = -P_i^m + P_i \tag{3a}$$
$$\tau_{Q_i} \dot{Q}_i^m = -Q_i^m + Q_i \tag{3b}$$

with $\tau_{P_i}$ and $\tau_{Q_i}$ the filters time constants; $P_i$ and $Q_i$ are the active and reactive power outputs of the $i$th DG.

TC layer is endowed with a virtual leader, labeled with index 0, that is, DG 0, able to supply voltage and frequency set-points $v_0$ and $\omega_0$ to a subset of DGs within the MG. Furthermore, each DG $i$ within the network $\forall i = 1, \ldots, N$, exchanges its information with the corresponding neighbors via onboard smart devices enabling the communication (see Fig. 1). Hence, the MG resembles a MAS, where each DG is an agent and distributed cooperative SC strategies can be applied to solve voltage regulation problem. This problem can be recast as a leader-tracking one, where the objective is to design $v_i^n$ in (2) such that the terminal voltage amplitude of each DG $v_i^{\text{out}}$ converges to the TC reference value, that is, $v_i^{\text{out}} \to v_0$, where

$$v_i^{\text{out}} = \sqrt{\left(v_i^{od}\right)^2 + \left(v_i^{oq}\right)^2}. \tag{4}$$

This latter implies that SC input $v_i^n$ has to guarantee that $v_i^{od} \to v_0$ due to $v_i^{oq} = 0$.

In the sequel, we first characterize the electrical interaction among DGs, provided by the power transmission lines in the physical layer connecting DGs and local loads, and, then, the communication interaction due to distributed SC, enabling connection among DGs in the cyber-space. The resulting double-layer MG structure can be modeled by exploiting the graph theory as follows [3].

### A. Communication Interaction

Interaction in the cyber-space among the $N$ DGs is conventionally modeled as directed graph $\mathcal{G}_N^c = \{\mathcal{V}_N^c, \mathcal{E}_N^c, A_N^c\}$, where $\mathcal{V}_N^c = 1, 2, \ldots, N$ is the set of $N$ interacting DGs, $\mathcal{E}_N^c \subseteq \mathcal{V}_N^c \times \mathcal{V}_N^c$ is the set of edges standing for direct and active communication links. $\mathcal{A}_N^c = [a_{ij}] \in \mathbb{R}^{N\times N}$ represents the adjacency matrix, whose elements are such that $a_{ij} = 1$ if there exists a communication channel from DG $j$ to DG $i$, and $a_{ij} = 0$ otherwise. Furthermore, it is possible to associate to the directed graph the degree matrix $\mathcal{D}_N^c = \text{diag}\{\Delta_1, \Delta_2, \ldots, \Delta_N\}$, where $\Delta_i = \sum_{j\in\mathcal{V}_N^c} a_{ij}\ \forall i$. Hence, the Laplacian matrix can be computed as $\mathcal{L} = \mathcal{D}_N^c - \mathcal{A}_N^c$. The presence of virtual DG 0 - mimicking the TC in providing reference frequency and voltage behavior $\omega_0$ and $v_0$- leads to an augmented directed graph $\mathcal{G}_{N+1}^c$ in the cyber-space. Therefore, a Pinning matrix $\mathcal{P} = \text{diag}\{p_1, p_2, \ldots, p_N\}$ is used to model the interaction among the $N$ DGs and the leader agent 0, whose entries are such that $p_i = 1$ if the leader information is directly available for the $i$th DG, 0 otherwise. Furthermore, $\mathcal{N}_i^c = \{j : (i, j) \in \mathcal{E}_{N+1}^c\}$ denotes the set of neighbors of the $i$th DG.

*Assumption 1:* There exists a path in $\mathcal{G}_{N+1}^c$ from DG $i$ in $\mathcal{G}_N^c$ to node 0 $\forall i \in \mathcal{V}_N^c$. This means that the virtual DG 0 is globally reachable in $\mathcal{G}_{N+1}^c$ and, hence, every DG can obtain TC references directly or indirectly.

### B. Electrical Interaction

The physical interaction among the electrical entities, provided by power transmission lines, can be also described by leveraging graph theory. Specifically, given $N + M$ electrical units, their physical interaction can be modeled via the connected and complex-weighted graph $\mathcal{G}^e = \{\mathcal{V}^e, \mathcal{E}^e, \mathcal{A}^e\}$, where $\mathcal{V}^e = 1, 2, \ldots, N + M$ is the set of electrical entities, $\mathcal{E}^e \subseteq \mathcal{V}^e \times \mathcal{V}^e$ is the set of physical edges, that is, the impedences of the power lines, and $\mathcal{A}^e = [a_{\rho k}] \in \mathbb{C}^{(N+M)\times(N+M)}$ is the electrical adjacency matrix, whose complex entries stand for the admittance between different buses. For instance, the generic $a_{\rho k} = Y_{\rho k} = G_{\rho k} + jB_{\rho k} \in \mathbb{C}$, where $G_{ik} \in \mathbb{R}$ and $B_{ik} \in \mathbb{R}$ are the conductance and susceptance, respectively, while $j$ is used for the imaginary unit (with a little abuse of notation). Hence, $Y_{\rho k} = 0$ means that there is no power line between $\rho$th and $k$th electrical entities within the grid. Similarly, $\mathcal{N}_\rho^e = \{k : k \in \mathcal{V}^e, k \neq \rho, Y_{\rho k} \neq 0\}$ refers to the neighboring electrical set of the $\rho$th electrical unit. Moreover, it follows $G_{\rho\rho} = \sum_{k\in\mathcal{N}_\rho^e} G_{\rho k}$ and $B_{\rho\rho} = \sum_{k\in\mathcal{N}_\rho^e} B_{\rho k}$.

*Assumption 2:* The electrical network topology $\mathcal{G}^e$ is characterized by lossless power transmission lines, that is, $G_{\rho k} = 0$ and $Y_{\rho k} = jB_{\rho k}\ \forall \rho \in \mathcal{V}^e,\ k \in \mathcal{N}_\rho^e$.

Assumption 2 is common in power system analysis. Interested readers may refer to [3] and [33] and references therein for more details.

In light of Assumption 2 and power balance equations, the active and reactive injected power for the $\rho$th electrical bus are given by [34]

$$\hat{P}_\rho = \sum_{k\in\mathcal{N}_\rho^e} v_\rho v_k B_{\rho k} \sin\left(\delta_\rho - \delta_k\right) \tag{5a}$$

$$\hat{Q}_\rho = v_\rho^2 B_{\rho\rho} - \sum_{k\in\mathcal{N}_\rho^e} v_\rho v_k B_{\rho k} \cos(\delta_i - \delta_k) \tag{5b}$$

where $v_\rho$ and $\delta_\rho$ are the voltage and phase angle of the $\rho$th electrical bus.

The ZIP load model is employed to describe the behavior of the generic load located at the $\rho$th bus, that is [35]

$$P_{L\rho} = P_{1_\rho} v_\rho^2 + P_{2_\rho} v_\rho + P_{3_\rho} \tag{6a}$$

$$Q_{L\rho} = Q_{1_\rho} v_\rho^2 + Q_{2_\rho} v_\rho + Q_{3_\rho} \tag{6b}$$

with pairs $(P_\rho, Q_{1_\rho})$, $(P_{2_\rho}, Q_{2_\rho})$ and $(P_{3_\rho}, Q_{3_\rho})$ standing for the nominal constant impedance, current and power loads, respectively. Based on (5a)–(6b), we finish up with the following total active and reactive power output of the $i$th DG:

$$P_i = \sum_{\rho\in\mathcal{N}_i^e} P_{L_\rho} + \sum_{\rho\in\mathcal{N}_i^e} \hat{P}_\rho, \quad i = 1, 2 \ldots, N \tag{7a}$$

$$Q_i = \sum_{\rho\in\mathcal{N}_i^e} Q_{L_\rho} + \sum_{\rho\in\mathcal{N}_i^e} \hat{Q}_\rho, \quad i = 1, 2 \ldots, N. \tag{7b}$$

*Assumption 3:* The instantaneous power flowing throughout the grid is bounded everywhere, that is, there exist known positive constants $\Pi^P$ and $\Pi^Q$ such that

$$|P_i| \leq \Pi^P,\ |Q_i| \leq \Pi^Q, \quad i = 1, 2, \ldots, N.$$

Note that, Assumption 3 is always satisfied due to bounded operating range of the inverter voltages and currents [32].

This study focuses on the voltage SC, where the objective is to set $v_i^n$ in (2) in order to regulate the voltage of each DG $i\ \forall i = 1, 2, \ldots, N$, to nominal value and compensate

natural deviations induced by droop-based PC. Specifically, a novel distributed SC strategy is introduced through this manuscript, where a novel DETM is suggested to mitigate the communication burden and significantly reduce the unnecessary sample-data transmission.

## III. Dynamic Event-Triggered PID-Like Control Using Artificial Delays

Here, we design the secondary voltage control $v_i^n$ in (2) able to synchronize all DGs voltage $v_i^{\text{out}}$ to the reference voltage $v_0$, which implies the synchronization of the direct term $v_i^{od}$ $\forall i = 1, 2, \ldots, N$. This control problem, which can be recast as a leader-tracking one, is here tackled by designing a novel distributed DETM able to reduce the communication burden and saving limited network resources. To this end, we first derive the voltage dynamics of the $i$th DG. Note that, for sake of brevity, throughout this article we omit the dependence on $d-q$ reference frame of $v_i^{od}$ in (2), that is, $v_i^{od} = v_i$.

By differentiating (2) and taking into account (3b), we derive the following simplified second-order model:

$$k_{v_i}\ddot{v}_i(t) + \dot{v}_i(t) + n_i^Q \dot{Q}_i^m + \hat{u}_i(t) = 0 \tag{8}$$

where $\hat{u}_i(t) = \dot{v}_i^n$ is the $i$th DG control input generating PC voltage reference to be designed later. By leveraging state-space formalism, (8) leads to

$$\dot{x}_i(t) = \begin{bmatrix} 0 & 1 \\ 0 & 0 \end{bmatrix} x_i(t) + \begin{bmatrix} 0 \\ -\frac{1}{k_{v_i}} \end{bmatrix} \big(\hat{u}_i(t) + w_i(t)\big) \tag{9}$$

where $x_i(t) = [v_i(t) \;\; \dot{v}_i(t)]^\top \in \mathbb{R}^2$ is the voltage state vector, while $w_i(t) = h(t, v_i, Q_i, Q_i^m) \in \mathbb{R}$ is the disturbance taking into account the voltage deviation induced by PC, with $h(t, v_i, Q_i, Q_i^m) = -\dot{v}_i(t) - n_i^Q \dot{Q}_i^m$.

*Remark 1:* Note that, Assumption 3 ensures the boundedness property for the term $w_i(t)$ in (9) [3]. It means that

$$\exists \quad \Pi \in \mathbb{R}^+ \quad : |w_i(t)| \leq \Pi \; \forall i = 1, 2, \ldots, N.$$

On the other hand, the leading dynamics of the reference generator DG 0 emulating the TC layer can be modeled as the following autonomous system:

$$\dot{x}_0(t) = \begin{bmatrix} 0 & 1 \\ 0 & 0 \end{bmatrix} x_0(t) \tag{10}$$

where $x_0(t) = [v_0(t) \; \dot{v}_0(t)]^\top \in \mathbb{R}^2$ is the leader DG 0 reference state vector. Then, for the generic $i$th DG, the synchronization error can be presented as

$$e_i(t) = v_i(t) - v_0(t), \quad i = 1, 2, \ldots, N. \tag{11}$$

Now, the SC control input $\hat{u}_i(t)$ in (9) is designed such that

$$\lim_{t\to\infty} \|e_i(t)\| = 0 \quad \forall i \tag{12}$$

while ensuring the communication resources saving. To achieve this aim, we propose the following three-steps procedure: 1) introduction of a distributed PID voltage controller $u_i(t)$ which, although leveraging a continuous information sharing over the communication network, is practical to be implemented thanks to the finite-time difference implementation of the derivative action; 2) sampled-data implementation of the previous designed controller $u_i(t)$ in order to obtain a digital control scheme, hence ensuring a preliminary reduction of transmitted control signal; and 3) design of the dynamic event-triggering rule to further decrease the communication network workload from the controller to actuator, while saving its limited resources [36]. In the sequel, we describe all the design steps of the proposed control architecture, which is schematized in Fig. 1, with the aim to clearly highlight how unnecessary sampled-data transmission is mitigated.

*1) Step 1:* From (11), the control $u_i(t)$ is designed as a distributed continuous-time PID controller weighting the networked shared information as

$$\begin{aligned} u_i(t) = \bar{k}_P \sum_{j\in\mathcal{N}_i^c} a_{ij}\big(e_i(t) - e_j(t)\big) \\ + \bar{k}_I \sum_{j\in\mathcal{N}_i^c} a_{ij} \int_0^t \big(e_i(s) - e_j(s)\big)\, ds \\ + \bar{k}_D \sum_{j\in\mathcal{N}_i^c} a_{ij}\big(\dot{e}_i(t) - \dot{e}_j(t)\big) \end{aligned} \tag{13}$$

where $\bar{k}_P$ is the proportional control gain, $\bar{k}_I$ is the integral control gain and $\bar{k}_D$ is the derivative control gain; and $a_{ij}$ is the generic element of the adjacency matrix (see Section II-A). Note that, in general control engineering practice there is a widely exploitation of PID controllers due to their ability in providing fast response to the transient phase while reducing steady-state deviations [29], [37]. However, this class of controllers depends on the derivative of the output, hardly to be measured in practice [24], [38]. To deal with this problem, according to [29], we transform the control input in (13) in a distributed PIR controller by using the following finite-difference approximations for the derivative terms, that is:

$$\begin{aligned} \dot{e}_i(t) \approx \bar{e}_i(t) = \frac{e_i(t) - e_i(t-h)}{h} \\ \dot{e}_j(t) \approx \bar{e}_j(t) = \frac{e_j(t) - e_j(t-h)}{h} \end{aligned} \tag{14}$$

with $i, \; j = 1, 2, \ldots, N$ and $h > 0$. Hence, by exploiting (14), the distributed PIR controller for the $i$th DG has the following form:

$$\begin{aligned} u_i(t) = k_P \sum_{j\in\mathcal{N}_i^c} a_{ij}\big(e_i(t) - e_j(t)\big) \\ + k_I \sum_{j\in\mathcal{N}_i^c} a_{ij} \int_0^t \big(e_i(s) - e_j(s)\big)\, ds \\ + k_D \sum_{j\in\mathcal{N}_i^c} a_{ij}\big(e_i(t-h) - e_j(t-h)\big) \end{aligned} \tag{15}$$

where the control gains, based on the finite-difference method, can be expressed as

$$k_P = \bar{k}_P + \frac{\bar{k}_D}{h}, \quad k_I = \bar{k}_I, \quad k_D = -\frac{\bar{k}_D}{h}. \tag{16}$$

Note that, Euler approximation in (14) is commonly used to replace a derivative-dependent controller as in (13) with a

delay-dependent one as in (15). If control law (13) stabilizes the system, then the stabilization is also achieved by (15) for sufficiently small $h > 0$ [38].

*2) Step 2:* To ensure a preliminary reduction of communication resources, here we propose a sampled-data implementation of the distributed PIR controller (15). To this end, we assume that the tracking error $e_i(t)$ is available only at the discrete-time instants $t_k = kh$, where $k \in \mathbb{N}_0$ and $h > 0$ is the sampling period. Specifically, given (14), to derive a digital implementation of the controller (13), according to [24], we use the following approximations for $t \in [t_k, t_{k+1}),\ k \in \mathbb{N}_0$:

$$\begin{aligned} e_i(t) &\approx \bar{e}_i(t) = \bar{e}_i(t_k) \\ \int_0^t e_i(s)\,ds &\approx \int_0^{t_k} \bar{e}_i(s)\,ds \approx \sum_{s=0}^{k-1} \int_{t_s}^{t_{s+1}} \bar{e}_i(s)\,ds \\ &\approx \sum_{s=0}^{k-1} \int_{t_s}^{t_{s+1}} \bar{e}_i(t_s)\,ds \\ &= h \sum_{s=0}^{k-1} \bar{e}_i(t_s) \\ \dot{e}_i(t) &\approx \dot{\bar{e}}_i(t) \approx \dot{\bar{e}}_i(t_k) = \frac{\bar{e}_i(t_k) - \bar{e}_i(t_{k-1})}{h}. \end{aligned} \tag{17}$$

By leveraging (17), (15) can be recast in sampled-data fashion as

$$\begin{aligned} u_i(t) = \bar{k}_P &\sum_{j \in \mathcal{N}_i^c} a_{ij}\big(\bar{e}_i(t_k) - \bar{e}_j(t_k)\big) \\ &+ \bar{k}_I h \sum_{j \in \mathcal{N}_i^c} a_{ij} \sum_{s=0}^{k-1} \big(\bar{e}_i(t_s) - \bar{e}_j(t_s)\big) \\ &+ \bar{k}_D \sum_{j \in \mathcal{N}_i^c} a_{ij}\big(\dot{\bar{e}}_i(t_k) - \dot{\bar{e}}_j(t_k)\big). \end{aligned} \tag{18}$$

We further present $u_i(t)$ in the following form:

$$\begin{aligned} u_i(t) &= \bar{k}_P \sum_{j \in \mathcal{N}_i^c} a_{ij}\big(\bar{e}_i(t_k) - \bar{e}_j(t_k)\big) + \bar{k}_I h \sum_{j \in \mathcal{N}_i^c} a_{ij} \sum_{s=0}^{k-1} \big(\bar{e}_i(t_s) - \bar{e}_j(t_s)\big) \\ &\quad + \bar{k}_D \sum_{j \in \mathcal{N}_i^c} a_{ij}\left(\left(\frac{\bar{e}_i(t_k) - \bar{e}_i(t_{k-1})}{h}\right) - \left(\frac{\bar{e}_j(t_k) - \bar{e}_j(t_{k-1})}{h}\right)\right) \\ &= k_P \sum_{j \in \mathcal{N}_i^c} a_{ij}\big(\bar{e}_i(t_k) - \bar{e}_j(t_k)\big) + k_I h \sum_{j \in \mathcal{N}_i^c} a_{ij} \sum_{s=0}^{k-1} \big(\bar{e}_i(t_s) - \bar{e}_j(t_s)\big) \\ &\quad + k_D \sum_{j \in \mathcal{N}_i^c} a_{ij}\big(\bar{e}_i(t_{k-1}) - \bar{e}_j(t_{k-1})\big), \quad t \in \big[t_k, t_{k+1}),\ k \in \mathbb{N}_0 \end{aligned} \tag{19}$$

with $k_P, k_I$ and $k_D$ defined in (16).

*3) Step 3:* To further reduce the network workload demanded by the distributed sampled-data PID control, we enrich it with a DETM. To this aim, inspired by [17], we first introduce the following $i$th internal dynamic variable associated with DG $i$ within the MG:

$$\dot{\lambda}_i(t) = -\theta \lambda_i(t) + \sigma\beta|u_i(t_k)|^2 - \beta|\epsilon_i(t_k)|^2, \quad t \in [t_k, t_{k+1}) \tag{20}$$

with design parameters $\theta > 0,\ \sigma \in (0, 1),\ \beta > 0$ and $\lambda_i(t_0) = \lambda_{i,0} > 0$; the term $\epsilon_i$ is defined as

$$\epsilon_i(t_k) = u_i(t_k) - \hat{u}_i(t_k) \tag{21}$$

where $\hat{u}_i(t_k)$ is the last effective control input sent, at $t_k$, to the $i$th DG actuator.

With the aim of ensuring the voltage stability of the whole closed-loop network, the idea of the proposed DETM is not to require that $\beta(\sigma(u_i(t_k)|^2 - |\epsilon_i(t_k)|^2)$ is always non-negative, but to ensure that it is non-negative in average [17]. Accordingly, we design the control action $\hat{u}_i(t)$ in (8) according to the following rule:

$$\hat{u}_i(t) = \hat{u}_i(t_k) = \begin{cases} u_i(t_k), & \text{if (23) is true} \\ \hat{u}_i(t_{k-1}), & \text{otherwise} \end{cases} \tag{22}$$

$$\gamma\lambda_i(t_k) + \sigma\beta|u_i(t_k)|^2 - \beta|\epsilon_i(t_k)|^2 < 0 \tag{23}$$

where $u_i(t_k)$ is the control action due to sample-data controller in (20) at the time $t_k$, while $\gamma > 0$ is an additional design parameter of the proposed DETM. Given (20), this design choice implies voltage stability to guarantee when $\lambda_i(t)$ is non-negative $\forall t \geq 0$, according to the following lemma.

*Lemma 3:* Let $\sigma \in (0, 1), \lambda_{i,0}, \gamma, \beta \in \mathbb{R}_0^+$ and let $u_i,\ \lambda_i$ and $\epsilon_i$ defined in (19), (20), and (21). Then, for all $t \in [0, t_\infty)$, the DETM in (22) and (23) ensures $\gamma\lambda_i(t_k) + \sigma\beta|u_i(t_k)|^2 - \beta|\epsilon_i(t_k)|^2 \geq 0$ and $\lambda_i(t) \geq 0$, for all $i = 1, 2, \ldots, N$.

*Proof:* By construction, mechanism (22) ensures that $\forall t \in [0, t_\infty),\ \gamma\lambda_i(t_k) + \sigma\beta|u_i(t_k)|^2 - \beta|\epsilon_i(t_k)|^2 \geq 0,\ i = 1, 2, \ldots, N$, where $t_\infty$ is the limit of $t_k = kh$ when $k \to +\infty$. If $\beta = 0$, then $\lambda_i(t_k) \geq 0$. On the other hand, if $\beta \neq 0$ we have $\sigma\beta|u_i(t_k)|^2 - \beta|\epsilon_i(t_k)|^2 \geq -\gamma\lambda_i(t_k)$. Then, from (20), we get $\dot{\lambda}_i(t) \geq -\theta\lambda_i(t) - \gamma\lambda_i(t_k),\quad t \in [t_k, t_{k+1})$, for all $t \in [0, t_\infty)$, with $\lambda(0) = \lambda_0 \geq 0$. Comparison lemma [39] guarantees $\lambda(t) \geq 0\ \forall t \in [0, t_\infty)$. ■

*Remark 2:* Step 1) reveals the potential of artificial delay approach, usually used for stabilization of some systems via the introduction of a delay in the feedback [40]. It is referred as *artificial delay* approach aiming to stability of some classes of system that cannot be stabilized by memoryless static output-feedbacks which, instead, can be stabilized by using output-feedbacks with intentionally introduced delays (see, e.g., [41] and references therein). Indeed, (14) replaces the derivative-dependent controller (13) with a delay-dependent one in (15). That is, the delay-induced stability is guaranteed for small $h > 0$ if the derivative-dependent control stabilizes the system [42].

*Remark 3:* The discrete-time DETM in (21)–(23) ensures that Zeno behavior is automatically ruled out. By choosing a small enough $h > 0$, one can find control gains (according to Lemma 4 below) before starting to enlarge sampling period by DETM (22) and (23). This guarantees that, in the worst case, the sampled-data implementation of the proposed controller, carried-out through Step 2), leads to minimum interevent time (MIET) such that MIET $= h > 0$, with $h$ the sampling period and $t_k = kh,\ k \in \mathbb{N}_0$, the discrete-time instants at which tracking errors $e_i\ \forall i = 1, \ldots, N$, are available. It is worth noting that the exploitation of auxiliary internal variable $\lambda_i(t)$, with its own dynamics, allows us moving from

*static* ETM to a *dynamic* one, which is highly beneficial in terms of larger interevent times due to its non-negative property (see Lemma 3) [43]. Indeed, due to $\lambda_i(t)$ (see [17, Proposition 2.3.]), the MIET cannot be smaller than the one guaranteed by classical static ET mechanism (obtained when $\gamma = 0$). In doing so, larger values of $\gamma$ result larger values of the MIET. This also guarantees that, compared to ET in [26], DETM in (22) and (23) with additional tuning parameter $\gamma \geq 0$ may allow to further reduce workload.

## IV. Stability Analysis

To prove how the proposed distributed PIR control, embedded with DETM (22) and (23), can synchronize the DGs output voltage $v_i$ to the references state $v_0$ (hence solving the control objective (12) with limited communication resources), we first introduce a proposition, instrumental for the LK stability analysis which we perform in this section.

*Proposition 1 [24], [41]:* For the $i$th DG, the error derivative $\dot{\tilde{e}}_i(t)$ defined in (17) satisfies

$$\dot{\tilde{e}}_i(t) = \dot{e}_i(t) + \kappa_i(t), \quad \kappa_i(t) = \int_{t-h}^{t} \frac{t-h-s}{h} \ddot{e}_i(s)\, ds \ \forall i. \tag{24}$$

*Proof:* Following arguments in [44], by exploiting Taylor's expansion with the remainder in the integral form, it yields

$$e_i(t-h) = e_i(t) + \dot{e}_i(t)h - \int_{t-h}^{t} (t-h-s)\ddot{e}_i(s)\, ds. \tag{25}$$

Proposition 1 can be obtained by recasting terms in (25), that is:

$$\dot{\tilde{e}}_i(t) = \frac{e_i(t) - e_i(t-h)}{h} = \dot{e}_i(t) + \int_{t-h}^{t} \frac{t-h-s}{h} \ddot{e}_i(t). \tag{26}$$

■

### A. Closed-Loop MG Network

Introduce the following enlarged vectors: $\zeta(t) = [e_1(t), e_2(t), \ldots, e_N(t)] \in \mathbb{R}^N$, $\bar{\zeta}(t) = [\dot{\tilde{e}}_1(t), \dot{\tilde{e}}_2(t), \ldots, \dot{\tilde{e}}_N(t)] \in \mathbb{R}^N$, $\hat{\zeta}(t) = [(t-t_k)\bar{e}_1(t_k) + h\sum_{s=0}^{k-1} \bar{e}_1(t_s), \ (t-t_k)\bar{e}_2(t_k) + h\sum_{s=0}^{k-1} \bar{e}_2(t_s) \ldots, \ (t-t_k)\bar{e}_N(t_k) + h\sum_{s=0}^{k-1} \bar{e}_N(t_s)] \in \mathbb{R}^N$, $\chi(t) = [\zeta^\top(t)\ \bar{\zeta}^\top(t)\ \hat{\zeta}^\top(t)] \in \mathbb{R}^{3N\times 3N}$ with $t \in [t_k, t_{k+1}),\ k \in \mathbb{N}_0$.

Moreover, denote the errors due to sampling as

$$\begin{aligned} \varsigma(t) &= \chi(t_k) - \chi(t) \in \mathbb{R}^{3N} \\ \varphi(t) &= \bar{\zeta}(t_k) - \bar{\zeta}(t) \in \mathbb{R}^N, \quad t \in [t_k, t_{k+1}),\ k \in \mathbb{N}_0. \end{aligned} \tag{27}$$

Furthermore, given Proposition 1, we define the additional augmented vector $\varkappa(t) = [\kappa_1(t), \kappa_2(t), \ldots, \kappa_N(t)] \in \mathbb{R}^N$.

In light of the above notation, the distributed digital-controller input vector $\bar{u}(t) = [u_1(t),\ u_2(t), \ldots, u_N(t)] \in \mathbb{R}^N$ can be rewritten as

$$\begin{aligned} \bar{u}(t) = &\begin{bmatrix} \bar{k}_P\mathscr{H} & \bar{k}_D\mathscr{H} & \bar{k}_I\mathscr{H} \end{bmatrix}\chi(t) + \begin{bmatrix} \bar{k}_P\mathscr{H} & 0_{N\times N} & \bar{k}_I\mathscr{H} \end{bmatrix}\varsigma(t) \\ &+ \bar{k}_D\mathscr{H}(\varkappa(t) + \varphi(t)), \quad t \in [t_k, t_{k+1}) \end{aligned} \tag{28}$$

with $\mathscr{H} = \mathscr{L} + \mathscr{P}$, where $\mathscr{L}$ and $\mathscr{P}$ are the Laplacian and Pinning matrices defined in Section II-A.

Given (8), (10), and (28), the closed-loop system under the action of DETM (22) and (23) can be derived as

$$\begin{aligned} \dot{\chi}(t) = &\Phi\chi(t) + \mathscr{A}_1\varsigma(t) + \mathscr{A}_2(\varkappa(t) + \varphi(t)) \\ &+ \mathscr{B}(\bar{w}(t) + \varepsilon(t)) \end{aligned} \tag{29}$$

with matrices

$$\begin{aligned} \Phi &= \begin{bmatrix} 0_{N\times N} & I_{N\times N} & 0_{N\times N} \\ \bar{k}_P\bar{B}\mathscr{H} & \bar{k}_D\bar{B}\mathscr{H} & \bar{k}_I\bar{B}\mathscr{H} \\ I_{N\times N} & 0_{N\times N} & 0_{N\times N} \end{bmatrix} \\ \mathscr{A}_1 &= \begin{bmatrix} 0_{N\times N} & 0_{N\times N} & 0_{N\times N} \\ \bar{k}_P\bar{B}\mathscr{H} & 0_{N\times N} & \bar{k}_I\bar{B}\mathscr{H} \\ 0_{N\times N} & 0_{N\times N} & 0_{N\times N} \end{bmatrix} \\ \mathscr{A}_2 &= \begin{bmatrix} 0_{N\times N} \\ \bar{k}_D\bar{B}\mathscr{H} \\ 0_{N\times N} \end{bmatrix}, \quad \mathscr{B} = \begin{bmatrix} 0_{N\times Nr} \\ \bar{B} \\ 0_{N\times N} \end{bmatrix} \\ \bar{B} &= -\mathrm{diag}\left\{\frac{1}{k_{v1}}, \frac{1}{k_{v2}}, \ldots, \frac{1}{k_{vN}}\right\} \end{aligned} \tag{30}$$

and enlarged vectors $\varepsilon(t) = [\epsilon_1(t),\ \epsilon_2(t),\ \ldots,\ \epsilon_N(t)] \in \mathbb{R}^N$ and $\bar{w}(t) = [w_1(t), w_2(t), \ldots, w_N(t)] \in \mathbb{R}^N$, with $\epsilon_i$ and $w_i(t)$ defined in (21) and (9), respectively.

Note that, the MG closed-loop system with continuous controller (13) has the following form:

$$\dot{\chi}(t) = \Phi\chi(t) + \mathscr{B}\bar{w}(t) \tag{31}$$

and satisfies the following lemma.

*Lemma 4:* Let $\mu_i$, $i = 1, \ldots, N$ the $i$th eigenvalue of matrix $\bar{B}\mathscr{H}$. Given a decay rate $\bar{\alpha} > 0$, under Assumption 1, by choosing control gains in (13) as

$$\bar{k}_D > 0, \quad \bar{k}_P > 0 \quad \frac{\bar{k}_I}{\bar{k}_D} > \max_i\{\bar{k}_P\mu_i\} \tag{32}$$

if there exists a positive definite matrix $P \in \mathbb{R}^{3N\times 3N}$ and a positive scalar $c$ satisfying the following LMI:

$$\begin{bmatrix} P\Phi + \Phi^\top P + \bar{\alpha}P + I_{3N} & P\mathscr{B} \\ \star & -c^2 I_{3N} \end{bmatrix} < 0 \tag{33}$$

then controller (13) exponentially stabilizes system (31).

*Proof:* Consider the Lyapunov function $V = \chi^\top(t)P\chi(t)$. By differentiating this latter along the trajectories of (31), we obtain

$$\dot{V} + \bar{\alpha}V = \chi^\top\Big(P\Phi + \Phi^\top P + \bar{\alpha}P\Big)\chi + 2\chi^\top P\mathscr{B}\bar{w}. \tag{34}$$

For the attenuation factor $c > 0$, we consider the following performance index:

$$J = \int_0^\infty \Big[\chi^\top(s)\chi(s) - c^2\bar{w}^\top(s)\bar{w}(s)\Big]\, ds.$$

According to [25], we are looking for conditions which guarantee that (31) is internally stable and has $L_2$ gain less than $c$, that is, that $\dot{V} + \chi^\top\chi - c^2\bar{w}^\top\bar{w} < 0$. Therefore, given (34), by adding and subtracting $\chi^\top\chi - c^2\bar{w}^\top\bar{w}$, we conclude that if LMI in (33) holds, then

$$\dot{V} + \bar{\alpha}V + \chi^\top\chi - c^2\bar{w}^\top\bar{w} \leq 0 \tag{35}$$

which guarantees the robust exponential stability of (31) with a decay rate $\bar{\alpha}$. Note that, the feasibility of (33) is ensured if and

only if $\Phi$ is a Hurwitz stable matrix. Therefore, it is required to select $\bar{k}_P$, $\bar{k}_D$ and $\bar{k}_I$ guaranteeing $\Phi < 0$. According to [45], the characteristic polynomial of $\Phi$ can be computed as

$$\begin{aligned}|\lambda I - \Phi| &= |\lambda I_N| \times \left|\lambda^2 I_N - \lambda \bar{k}_D \bar{B}\mathscr{H} - \bar{k}_P \bar{B}\mathscr{H} + \frac{1}{\lambda}\bar{k}_I \bar{B}\mathscr{H}\right| \\ &= |\lambda^3 I_N + \left(-\lambda^2 \bar{k}_D - \lambda \bar{k}_P + \bar{k}_I\right)\bar{B}\mathscr{H}|. \end{aligned} \tag{36}$$

Given the expression of $\bar{B}$ in (30), if Assumption 1 holds, $\bar{B}\mathscr{H}$ has no zero eigenvalues which we indicate with $\mu_i$ ($i = 1, \ldots, N$). Since $|\xi I_N + \bar{B}\mathscr{H}| = \prod_{i=1}^{N}(\xi + \mu_i)$ [45], (36) can be rewritten as

$$|\lambda I - \Phi| = \prod_{i=1}^{N}\left(\lambda^3 + \left(-\lambda^2 \bar{k}_D - \lambda \bar{k}_P + \bar{k}_I\right)\mu_i\right). \tag{37}$$

Therefore, control gains can be designed such that the roots of

$$p_{\mu_i}(\lambda) = \lambda^3 - \bar{k}_D \mu_i \lambda^2 - \bar{k}_P \mu_i \lambda + \bar{k}_I \mu_i \tag{38}$$

have a negative real part $\forall p_{\mu_i}$, $i = 1, \ldots, N$. Then, by exploiting Routh-Hurwitz criterion, (38) is Hurwitz stable $\forall i$ if (32) holds. Therefore, the statement is proven. ■

### B. Proof of Convergence

The voltage synchronization process of the entire closed-loop MG network (29) is ensured according to the following LMIs-based stability criteria.

*Theorem 1:* Consider the closed-loop voltage dynamics (29) under the action of distributed DET controller (22) and (23), whose control gains are tuned according to Lemma 4. Let Assumptions 1–3 hold. Given sampling period $h > 0$, decay rate $\alpha < \bar{\alpha}$ and positive parameters $\sigma \in (0, 1)$, $\beta$, $\theta$ and $\gamma$, if there exist positive definite matrices $P$, $S \in \mathbb{R}^{3N\times 3N}$, $W$, $Q$, $R \in \mathbb{R}^{N\times N}$ and a scalar $b > 0$ such that

$$\left[\begin{array}{c|cc} \Theta & \begin{array}{c}\Phi^\top\Gamma \\ \mathscr{A}_1^\top\Gamma \\ \mathscr{A}_2^\top\Gamma \\ \mathscr{A}_2^\top\Gamma \\ \mathscr{B}^\top\Gamma \\ \mathscr{B}^\top\Gamma\end{array} & \begin{array}{c}\sqrt{\sigma\beta e^{-2\alpha h}}\left[\bar{k}_P\mathscr{H} \;\; \bar{k}_D\mathscr{H} \;\; \bar{k}_I\mathscr{H}\right]^\top \\ \sqrt{\sigma\beta e^{-2\alpha h}}\left[\bar{k}_P\mathscr{H} \;\; 0_{N\times N} \;\; \bar{k}_I\mathscr{H}\right]^\top \\ \sqrt{\sigma\beta e^{-2\alpha h}}\bar{k}_D\mathscr{H}^\top \\ \sqrt{\sigma\beta e^{-2\alpha h}}\bar{k}_D\mathscr{H}^\top \\ O_{N\times N} \\ O_{N\times N}\end{array} \\ \hline \star & -\Gamma & 0_{3N\times N} \\ & \star & -I_{N\times N}\end{array}\right] < 0 \tag{39}$$

with

$$\Theta = \begin{bmatrix} P\Phi+\Phi^\top P+2\alpha P & P\mathscr{A}_1 & P\mathscr{A}_2 & P\mathscr{A}_2 & P\mathscr{B} & P\mathscr{B} \\ \star & -\frac{\pi^2}{4}S & 0_{3N\times N} & 0_{3N\times N} & 0_{3N\times N} & 0_{3N\times N} \\ \star & \star & -\frac{\pi^2}{4}h^2 Q & 0_{N\times N} & 0_{N\times N} & 0_{N\times N} \\ \star & \star & \star & -e^{-2\alpha h}R & 0_{N\times N} & 0_{N\times N} \\ \star & \star & \star & \star & -bI_{N\times N} & 0_{N\times N} \\ \star & \star & \star & \star & \star & -\beta e^{-2\alpha h}I_{N\times N} \end{bmatrix} \tag{40}$$

$$\Gamma = h^2 e^{2\alpha h}S + \begin{bmatrix} 0_{N\times N} & 0_{N\times N} & 0_{N\times N} \\ 0_{N\times N} & h^2\left(e^{2\alpha h}Q + \frac{1}{4}R\right) & 0_{N\times N} \\ 0_{N\times N} & 0_{N\times N} & 0_{N\times N} \end{bmatrix} \tag{41}$$

then, the voltage recovery is exponentially achieved with a decay rate $\alpha$ and a small enough $h > 0$.

*Proof:* Introduce the following additional vector:

$$\bar{\lambda}(t) = [\lambda_1(t), \; \lambda_2(t), \ldots, \lambda_N(t)] \in \mathbb{R}^N \tag{42}$$

with $\lambda_i$, $i = 1, \ldots, N$, defined as in (20). Note that, for sake of brevity, throughout the proof we omit the dependence on the time $t$ for all variables. Consider the following LK functional:

$$V = V_P + V_S + V_W + V_Q + V_R + V_{\bar{\lambda}} \tag{43}$$

where

$$\begin{aligned} V_P &= \chi^\top P \chi, \quad V_{\bar{\lambda}} = e^{-2\alpha(t-t_k)}\bar{\lambda} \\ V_S &= h^2 e^{2\alpha h}\int_{t_k}^{t} e^{-2\alpha(t-s)}\dot{\chi}(s)^\top S\dot{\chi}(s)\,ds \\ &\quad - \frac{\pi^2}{4}\int_{t_k}^{t} e^{-2\alpha(t-s)}\varsigma^\top(s)S\varsigma(s)\,ds \\ V_W &= \int_{t_k}^{t} e^{-2\alpha(t-s)}\dot{\tilde{\zeta}}^\top(s)W\dot{\tilde{\zeta}}(s)\,ds \\ &\quad - \frac{\pi^2}{4}\int_{t_k}^{t} e^{-2\alpha(t-s)}\varphi^\top(s)W\varphi(s)\,ds \\ V_Q &= h^2 e^{2\alpha h}\int_{t-h}^{t} e^{-2\alpha(t-s)}\frac{s-t+h}{h}\ddot{\zeta}^\top(s)Q\ddot{\zeta}(s)\,ds \\ V_R &= \int_{t-h}^{t} e^{-2\alpha(t-s)}\frac{(s-t+h)^2}{4}\ddot{\zeta}^\top(s)R\ddot{\zeta}(s)\,ds. \end{aligned} \tag{44}$$

We highlight that the functional $V(t)$ in (43) is positive due to Lemma 1, ensuring $V_S \geq 0$ and $V_W \geq 0$, and Lemma 3 guaranteeing $V_{\bar{\lambda}} > 0$. Note that, $V_R$ is exploited for the compensation of the approximation errors $\varkappa(t)$ as in (29).

Differentiating $V_P$ along the trajectories of (29), it yields

$$\begin{aligned} \dot{V}_P + 2\alpha V_P &= 2\chi^\top P\dot{\chi} + 2\alpha\chi^\top P\chi = \chi^\top\left(P\Phi + \Phi^\top P + 2\alpha P\right)\chi \\ &\quad + 2\chi^\top P\mathscr{A}_1\varsigma + 2\chi^\top P\mathscr{A}_2(\varkappa + \varphi) \\ &\quad + 2\chi^\top P\mathscr{B}(\bar{w} + \varepsilon). \end{aligned} \tag{45}$$

Moreover, by differentiating $V_S$ and $V_W$ along (29), we have

$$\begin{aligned} \dot{V}_S + 2\alpha V_S &= h^2 e^{2\alpha h}\dot{\chi}^\top S\dot{\chi} - \frac{\pi^2}{4}\varsigma^\top S\varsigma \\ \dot{V}_W + 2\alpha V_W &= \dot{\tilde{\zeta}}^\top W\dot{\tilde{\zeta}} - \frac{\pi^2}{4}\varphi^\top W\varphi. \end{aligned} \tag{46}$$

The derivative of $V_Q$ in (44) leads to

$$\begin{aligned} \dot{V}_Q + 2\alpha V_Q &= h^2 e^{2\alpha h}\ddot{\zeta}^\top Q\ddot{\zeta} \\ &\quad - he^{2\alpha h}\int_{t-h}^{t} e^{-2\alpha(t-s)}\ddot{\zeta}^\top(s)\; Q\ddot{\zeta}(s)\,ds. \end{aligned} \tag{47}$$

By employing Lemma 2 to deal with the integral term of (47), we obtain

$$\begin{aligned} \dot{V}_Q + 2\alpha V_Q &\leq h^2 e^{2\alpha h}\ddot{\zeta}^\top Q\ddot{\zeta} \\ &\quad - \left(\int_{t-h}^{t}\ddot{\zeta}(s)\;ds\right)^\top Q\left(\int_{t-h}^{t}\ddot{\zeta}(s)\;ds\right). \end{aligned} \tag{48}$$

Then, after differentiating (24), that is, $\ddot{\tilde{e}}_i(t) = \int_{t-h}^{t}([\ddot{e}_i(s)]/h)\,ds$, and considering its vector form

$$\dot{\tilde{\zeta}} = \int_{t-h}^{t}\frac{\ddot{\zeta}(s)}{h}\,ds \tag{49}$$

inequality (48) can be finally recast as

$$\dot{V}_Q + 2\alpha V_Q \leq h^2 e^{2\alpha h} \ddot{\zeta}^\top Q \ddot{\zeta} - h^2 \dot{\tilde{\zeta}}^\top Q \dot{\tilde{\zeta}}. \tag{50}$$

Furthermore, by differentiating $V_R$ along the trajectories of (29), we have

$$\dot{V}_R + 2\alpha V_R = \frac{h^2}{4} \ddot{\zeta}^\top R \ddot{\zeta} - \int_{t-h}^{t} e^{-2\alpha(t-s)} \frac{(s-t+h)}{2} \ddot{\zeta}^\top(s) R \ddot{\zeta}(s)\, ds \tag{51}$$

and by using Jensen inequality in Lemma 2 for the integral term, (51) can be rewritten as

$$\dot{V}_R + 2\alpha V_R \leq \frac{h^2}{4} \ddot{\zeta}^\top R \ddot{\zeta} - e^{-2\alpha h} \varkappa^\top R \varkappa. \tag{52}$$

Finally, by differentiating $V_{\tilde{\lambda}}$ in (44), it follows:

$$\dot{V}_{\tilde{\lambda}} + 2\alpha V_{\tilde{\lambda}} = e^{-2\alpha(t-t_k)} \dot{\tilde{\lambda}}. \tag{53}$$

Given Lemma 3, from (20), we have

$$\dot{\tilde{\lambda}} \leq \sigma\beta |\bar{u}(t_k)|^2 - \beta |\varepsilon(t_k)|^2, \quad t \in [t_k, t_{k+1}) \tag{54}$$

with $\bar{u}(t_k)$ defined in (28). Exploiting (54), (53) can be rewritten as

$$\dot{V}_{\tilde{\lambda}} + 2\alpha V_{\tilde{\lambda}} \leq e^{-2\alpha h} \Big( \sigma\beta \big| \bar{u}(t_k) \big|^2 - \beta \big| \varepsilon(t_k) \big|^2 \Big). \tag{55}$$

Summing up (45), (46), (50), (52), and (55), and choosing $W = h^2 Q$, we get

$$\begin{aligned} \dot{V} + 2\alpha V \leq\ & \chi^\top \Big( P\Phi + \Phi^\top P + \alpha P \Big) \chi + 2\chi^\top P \mathscr{A}_1 \varsigma \\ & + 2\chi^\top P \mathscr{A}_2 (\varkappa + \varphi) + 2\chi^\top P \mathscr{B} (\bar{w} + \varepsilon) \\ & + h^2 e^{2\alpha h} \dot{\chi}^\top S \dot{\chi} - \frac{\pi^2}{4} \varsigma^\top S \varsigma - \frac{\pi^2 h^2}{4} \varphi^\top Q \varphi \\ & + \ddot{\zeta}^\top \left[ h^2 \left( e^{2\alpha h} Q + \frac{1}{4} R \right) \right] \ddot{\zeta} - e^{-2\alpha h} \varkappa^\top R \varkappa \\ & + e^{-2\alpha h} \Big( \sigma\beta |\bar{u}(t_k)|^2 - \beta |\varepsilon(t_k)|^2 \Big) \quad t \in [t_k, t_{k+1}). \end{aligned} \tag{56}$$

Now, after introducing the enlarged vector $\xi^\top = [\chi^\top \ \varsigma^\top \ \varphi^\top \ \varkappa^\top \ \bar{w}^\top \ \varepsilon^\top] \in \mathbb{R}^{10N}$, inequality (56) can be rewritten as

$$\dot{V} + 2\alpha V - b\bar{w}^\top \bar{w} \leq \xi^\top \Theta \xi + \dot{\chi}^\top \Gamma \dot{\chi} + e^{-2\alpha h} \sigma\beta |\bar{u}(t_k)|^2 \tag{57}$$

for $t \in [t_k, t_{k+1})$, where $\Theta \in \mathbb{R}^{10N \times 10N}$ and $\Gamma \in \mathbb{R}^{3N \times 3N}$ are defined in (40) and (41), respectively. Taking into account (28) and (29), from Schur complement, if (39) holds, we have

$$\dot{V} + 2\alpha V - b\bar{w}^\top \bar{w} \leq 0 \quad t \in [t_k, t_{k+1}). \tag{58}$$

Therefore, the fulfillment of (39) implies that voltage recovery process is exponentially achieved with a decay rate $\alpha > 0$ and a $L_2$ gain $b$. ■

*Remark 4:* Theorem 1 provides the values of $\sigma$, $\beta$ and $h$ preserving the stability of the network. The decay rate $\alpha > 0$ can be tuned by appropriately choosing parameters $h$, $\sigma$ and $\beta$ guaranteeing the feasibility of (39). Furthermore, from Lemma 3, it follows that the larger $\lambda_{i,0}$ yields a larger interevent time [46]. Moreover, in light of Remark 3, for $\gamma > 0$ we have $\gamma\lambda_i(t_k) > 0\ \forall i$, meaning that the proposed mechanism can produce larger interevent times than a static triggering mechanism. Indeed, larger values of $\gamma$ lead to larger interevent times (see [17], [46] for more details).

*Remark 5:* From a NCS perspective, the proposed control design ensures, for each distributed controller $i$, the reduction of communication resources in the cyber-space while decreasing, at the same time, the workload between each controller and the related actuator. In doing so, distributed sampled-data controller (20) leverages periodic, rather than continuous, information exchanges among DGs, thus achieving a preliminary reduction of the communication network workload (even if in absence of triggering mechanism). Besides this latter crucial aspect, the benefit of deriving a discrete-time controller as in (20) lies in addressing one of the actual challenges in distributed control of MASs, which is related to the design of distributed sampled-data controllers [23]. Indeed, as many advanced communication networks only permit digital information dissemination, continuous interactions among agents are no longer valid in NCS as in MG applications. Therefore, the need of reevaluating conventional distributed continuous-time controllers in a sampled-data fashion is emerged [23]. Moreover, when combining (20) with (22) and (23), a further reduction in the actuator updates for each DG $i$ is achieved. This is more favorable when limited resources of the embedded control systems are considered [47].

## V. Numerical Analysis

To validate the effectiveness of the proposed strategy (20), (22), and (23) in solving voltage recovery problem in MG, here we consider the IEEE 14-bus test system working in islanded mode. Note that, according to the IEEE Standard 1547.4 [48], it is a common practise to properly modify the IEEE 14-bus test system, or even larger IEEE test systems, so to simulate a MG and validate the robustness of the proposed distributed control scheme, along with its scalability requirement (see, e.g., for more details [49], [50]). $N = 5$ DGs on buses 1, 2, 3, 6 and 8 are involved into the grid, along with $M = 9$ local loads and twenty power transmission lines, whose parameters are detailed in [51]. The communication topology, chosen such that Assumption 1 holds, is described by the set $\mathscr{E}^c_{N+1} = \{(0,1),(1,2),(2,3),(3,2),(2,4),(3,4),(4,5)\}$, where the leader information is directly available only for DG 1. Note that, since this manuscript deals with secondary voltage control, frequency responses will be not shown for the sake of brevity. However, we highlight that frequency time history is maintained within the operating range of $\omega_0 = 50$ $[Hz]$ and restored via the distributed controller proposed in [52]. This latter is involved in our simulation platform in order to test the proposed voltage control strategy in a realistic MG environment.

Simulations are performed by leveraging MATLAB/Simulink, while the feasibility of LMIs in Theorem 1 is verified via Yalmip Toolbox through SeDuMi solver. Lemma 4 has been exploited to select of $\bar{k}_P$, $\bar{k}_I$ and $\bar{k}_D$, which leads to $\bar{k}_P = 30$, $\bar{k}_I = 0.1$ and $\bar{k}_D = 10$. For $\alpha = 0.1$ and $\beta = 1$, we verify

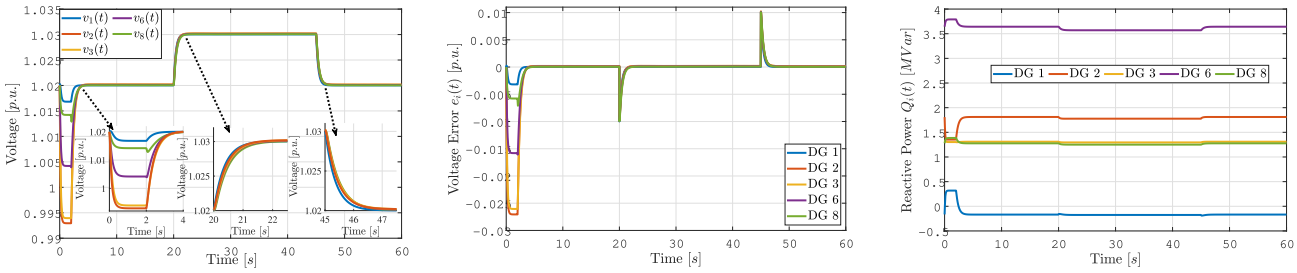


(a) (b) (c)

Fig. 2. Voltage recovery in *nominal scenario* under the distributed dynamic event-triggered PID-like controller. Time history of: (a) voltage $v_i(t)$, $i = \{1, 2, 3, 6, 8\}$; (b) voltage error $v_i(t) - v_0(t)$, $i = \{1, 2, 3, 6, 8\}$, and (c) reactive power $Q_i$, $i = \{1, 2, 3, 6, 8\}$.

the feasibility of LMIs in Theorem 1 in order to find the maximum values of $h$ and $\sigma$ ensuring the voltage stability. By solving these LMIs, the fulfillment of Theorem 1 is guaranteed for $h = 0.002$, $\sigma = 0.2$ and $b = 1.1578$. Note that, the approximation errors due to sampled-data implementation adversely affect the system. Indeed, if we use continuous control in (15), the maximum delay value is $h = 0.012$, while for sampled-data implementation we find a smaller sampling interval with maximum sampling period $h = 0.002$. Although it results a reduction of one order of magnitude for the upper bound of $h$, this is still beneficial for the communication network workload with limited resources as the interaction among agents becomes periodic rather than continuous. In the sequel, three different simulation scenarios are investigated, that is: 1) *nominal scenario*, where multiple changing in voltage set-point occur so to prove the tracking ability of the proposed controller; 2) *load changing scenario* where, besides changing in voltage set-points, there exist fluctuations in load demand; and 3) *plug and play scenario*, where plug-and-play phenomena are involved to disclose the robustness and the resilience of the control law (20), (22), and (23) in facing this more troublesome situation. Finally, to further confirm the effectiveness of the proposed approach, a comparison analysis w.r.t. the conventional static ET mechanism (obtained by selecting $\gamma = 0$) and the sampled-data controller in [29] is discussed.

### A. Case A—Nominal Scenario

Herein we consider multiple voltage reference set-points variations, that is: 1) at $t = 0$ $[s]$, only the PC works; 2) at $t = 2$ $[s]$, the SC is switched ON with $v_0 = 1.02$ $[p.u.]$; and 3) at $t = 20$ $[s]$, the voltage reference is changed as $v_0 = 1.03$ $[p.u.]$; *iv*) at $t = 45$ $[s]$, voltage set-point restores to the initial value $v_0 = 1.02$ $[p.u.]$.

Fig. 2 confirms the effectiveness of the proposed distributed DET PID-like controller in successfully solving the voltage restoration problem despite the presence of disturbances acting on DGs dynamics, multiple reference changes and deviations induced by PC. Specifically, from Fig. 2(a), it is shown that, prior to $t = 2$ $[s]$, where only PC is activated, each DG voltage is deviated from the desired set-point. Then, after activating the proposed DET controller at $t = 2$ $[s]$, voltage deviations are quickly compensated to the reference voltage value $v_0 = 1.02$ $[p.u.]$. Moreover, they are also restored after each reference changing happening at $t = 20$ $[s]$ and $t = 45$ $[s]$, respectively, thus allowing the voltage errors to approach to zero [see Fig. 2(b)]. For completeness, the time history of reactive power $Q_i$ of each DG, $i = 1, \ldots, 5$ has been reported in Fig. 2(c). Moreover, Fig. 5(a) shows the detail of the event-trigger time instants of each DG during the time interval $[2; 4]$ $[s]$ of this simulation scenario where, due to the DET mechanism, each DG is triggered aperiodically rather than continuously.

Hence, this latter figure highlights that the realize intervals are more frequent in transient phase while, after reaching steady-state, the number of sent control signal is smaller, thus confirming a reduction of the communication network workload.

### B. Case B—Load Changing Scenario

To prove the robustness of the proposed control law with respect to changing in load requests, here we consider a simulation scenario involving the following list of events: 1) at $t = 0$ $[s]$, only the PC works; 2) at $t = 2$ $[s]$, the voltage SC is switched ON with $v_0 = 1.02$ $[p.u.]$; 3) at $t = 20$ $[s]$, the voltage reference is changed as $v_0 = 1.03$ $[p.u.]$ and the nominal values of the loads increase by 30%; 4) at $t = 30$ $[s]$, there is an additional 20% of increase of the loads, until they restore their initial values at $t = 40$ $[s]$; and 5) at $t = 45$ $[s]$, voltage set-point restores to the initial value $v_0 = 1.02$ $[p.u.]$. Results in Fig. 3 illustrate the performance of the proposed control strategy in solving voltage regulation problem also in this more troublesome scenario where, besides voltage reference variations, there exist sudden changes in load demand. In particular, Fig. 3(a) shows that, for $t \in [0, 2)$ $[s]$, voltage deviations with respect to nominal value occur since SC is inactive and only droop-based PC is still working on each DG. Then, once the proposed SC is activated at $t = 2$ $[s]$, DGs voltages promptly react to restore the expected voltage value $v_0 = 1.02$ $[p.u.]$ imposed by the virtual DG 0 and, hence, voltage deviations induced by PC are successfully compensated. Thereafter, at $t = 20$ $[s]$, although voltage set-point changes as $v_0 = 1.03$ $[p.u.]$ and loads increase by 30%, the magnitude of the voltages of all DGs are quickly steered to the novel reference value as time goes by, meaning that voltage SC is achieved in spite of abrupt changes in the power

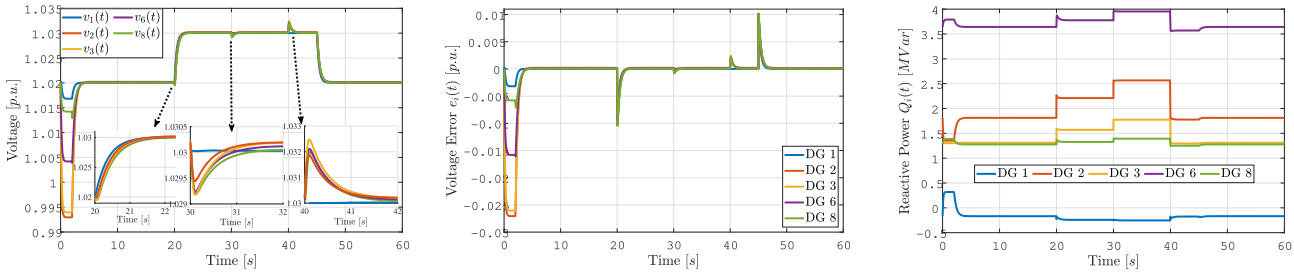


(a) (b) (c)

Fig. 3. Voltage recovery in *load changing scenario* under the distributed dynamic event-triggered PID-like controller. Time history of: (a) voltage $v_i(t)$, $i = \{1, 2, 3, 6, 8\}$; (b) voltage error $v_i(t) - v_0(t)$, $i = \{1, 2, 3, 6, 8\}$, and (c) reactive power $Q_i$, $i = \{1, 2, 3, 6, 8\}$.

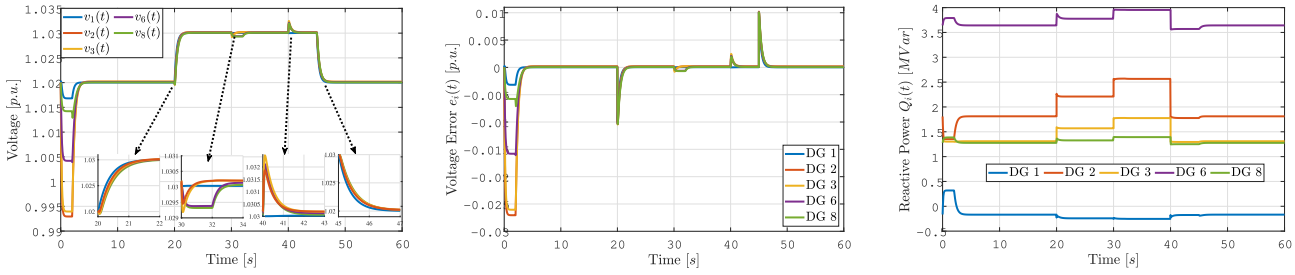


(a) (b) (c)

Fig. 4. Voltage recovery in *plug-and-play scenario* under the distributed dynamic event-triggered PID-like controller. Time history of: (a) voltage $v_i(t)$, $i = \{1, 2, 3, 6, 8\}$; (b) voltage error $v_i(t) - v_0(t)$, $i = \{1, 2, 3, 6, 8\}$, and (c) reactive power $Q_i$, $i = \{1, 2, 3, 6, 8\}$.

demand. The same good performance can be appreciated at $t = 30$ $[s]$ and at $t = 40$ $[s]$, where loads are increased by 20% and restored to the initial values, respectively. Finally, Fig. 3(a) also shows that, even if at $t = 45$ $[s]$ voltage set-point changes again as $v_0 = 1.02$ $[p.u.]$, synchronization of all DGs voltage $v_i(t)$ $\forall i$, is achieved very quickly under the action of distributed control law (22) and (23). Hence, each DG voltage error w.r.t. the set-point $v_0$ converges to zero in the steady-state, with small tolerable errors occurring during each transient phase when reference/load variations occur [Fig. 3(b)]. Moreover, realize intervals of each DG are shown in Fig. 5(b) for the time interval $[2; 4]$ $[s]$, that is, after reaching the first steady-state, thus highlighting how the proposed DET mechanism allows reducing the number of control inputs computed at single agent level, while alleviating communication network via an aperiodic control. For completeness, the time-history of the reactive-power $Q_i$ of each DG, has been reported in Fig. 3(c).

### C. Case C—Plug and Play Scenario

Here, a more challenging scenario, involving multiple complex phenomena to be properly managed in order to maintain MG stability, is considered. Specifically, the following simulation environment is emulated: 1) at $t = 0$ $[s]$, only the PC works; 2) at $t = 2$ $[s]$, the voltage SC is switched ON with $v_0 = 1.02$ $[p.u.]$; 3) at $t = 20$ $[s]$, the voltage reference is changed as $v_0 = 1.03$ $[p.u.]$ and an increasing of 30% of the loads nominal values occur; 4) at $t = 24$ $[s]$, DG 4 is unplugged; 5) at $t = 30$ $[s]$, the loads increase of an additional 20%; 6) at $t = 32$ $[s]$, DG 4 is plugged-in; 7) at $t = 40$ $[s]$, loads are restored to their nominal values; and 8) at $t = 45$ $[s]$, voltage set-point restores to the initial value $v_0 = 1.02$ $[p.u.]$. The effectiveness of the proposed control protocol in successfully achieving voltage synchronization is corroborated also in this worrying environment, as it is possible to observe in Fig. 4. It is worth noting that the robustness of the proposed control strategy w.r.t. communication links failures is also guaranteed via this simulation scenario. Indeed, as one DG within the power network fails, it also implies losses for the cyber links connected to the unplugged DGs [53]. It means that when DG 4 is unplugged at $t = 24$ $[s]$, communication links $(2, 4)$, $(3, 4)$ and $(4, 5)$ become useless. Although these plug-and-play phenomena, along with reference/load variations, may compromise MG voltage stability, the performance of the designed SC is confirmed and the voltage recovery problem can be considered as successfully solved also in this case [see Fig. 4(a)–(c)] with a good tradeoff between control performances and number of triggering instants [see Fig. 5(c)].

### D. Comparison With Conventional Static ET Control and Other State-of-the-Art Digital Controller

To further highlight the advantages of the proposed distributed DET PID-like controller in guaranteeing voltage restoration while reducing communication network workload, by considering the same simulation environment as in Case C, we first compare its performance with the one achievable via two kind controllers: 1) a conventional static event-triggered mechanism (resulting from (23) with $\gamma = 0$) and 2) the sampled-data controller recently suggested in our preliminary results in [29], where no ET

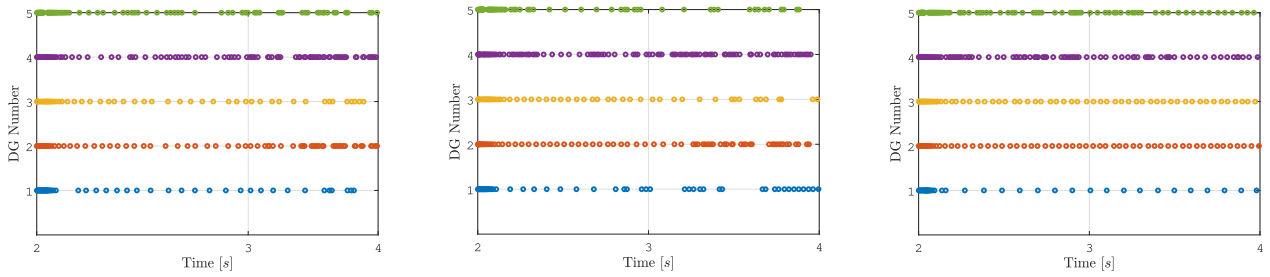


Fig. 5. Event-triggered time of each DG $i$, $i = 1, \ldots, 5$ under the distributed dynamic event-triggered PID-like controller: (a) *nominal scenario*; (b) *load changing scenario*; and (c) *plug-and-play scenario*.

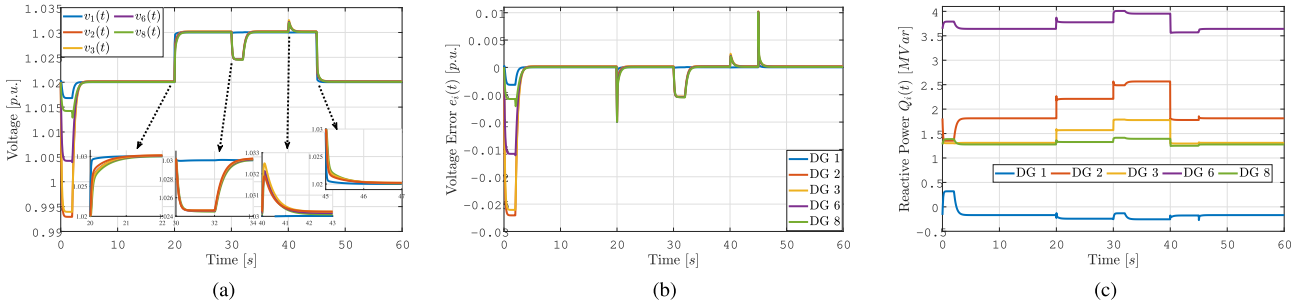


Fig. 6. Comparison analysis: Voltage recovery in *plug-and-play scenario* under the distributed static event-triggered PID-like controller. Time history of: (a) voltage $v_i(t)$, $i = \{1, 2, 3, 6, 8\}$; (b) voltage error $v_i(t) - v_0(t)$, $i = \{1, 2, 3, 6, 8\}$, and (c) reactive power $Q_i$, $i = \{1, 2, 3, 6, 8\}$.

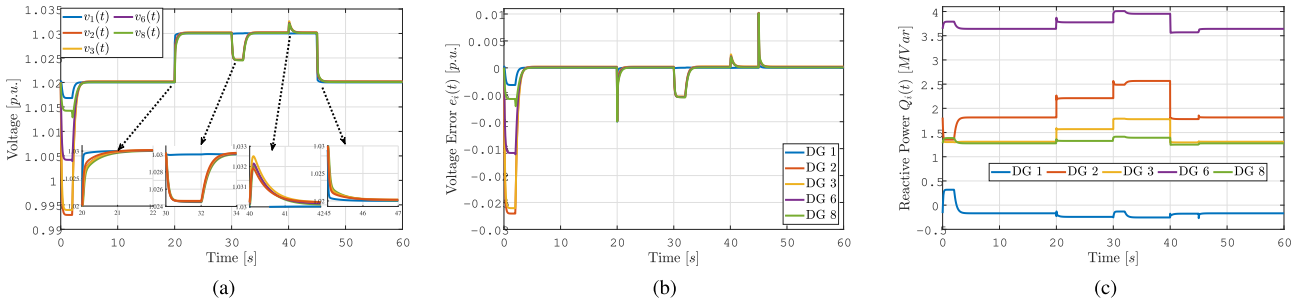


Fig. 7. Comparison analysis: Voltage recovery in *plug-and-play scenario* under the distributed sampled-data PID-like controller in [29]. Time history of: (a) voltage $v_i(t)$, $i = \{1, 2, 3, 6, 8\}$; (b) voltage error $v_i(t) - v_0(t)$, $i = \{1, 2, 3, 6, 8\}$, and (c) reactive power $Q_i$, $i = \{1, 2, 3, 6, 8\}$.

conditions are involved. The sampling period of the sampled-data controller in [29] is set to be $h = 0.002$, while the static triggered threshold is chosen as $\sigma = 0.2$ so to provide a fair comparison. Results in Figs. 6 and 7 highlight the performance of the two alternative controllers. Besides a slight improvement in transient performances, ensured by the proposed DET-based distributed controller, it is crucial to note the significant reduction we ensure into the number of sent control signals at single agent level. Comparison among the three controllers in terms of total trigger times is shown in Fig. 8. More in details, by considering a simulation time interval of 60 $[s]$, each DG units under controller in [29] computes $60/h + 1 = 30001$ control signals. Conversely, the total number of trigger times for DG $i$, with $i = 1, \ldots, 5$ under static ET mechanism are 1451, 1997, 1522, 2615 and 2700, respectively. Although the crucial reduction resulting from the static ET, our DET

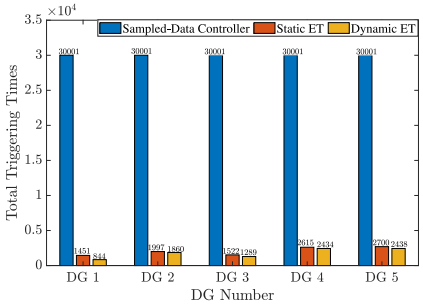


Fig. 8. Total trigger times of three secondary controllers: Sampled-data controller in [29] (blue bar), static ET (red bar), and proposed DET (yellow bar).

mechanism allows to further decrease the number of the control signals computed by each DG $i$, whose values are 844, 1860, 1289, 2434 and 2438, respectively. This confirms

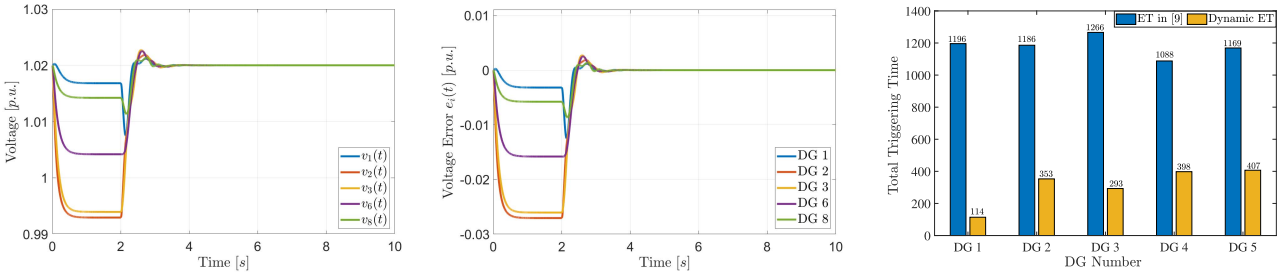


(a) (b) (c)

Fig. 9. Comparison analysis: Voltage recovery in *nominal scenario* under the ETC in [11]. Time history of: (a) voltage $v_i(t),\ i = \{1, 2, 3, 6, 8\}$; (b) voltage error $v_i(t) - v_0(t),\ i = \{1, 2, 3, 6, 8\}$, and (c) total trigger times of ETC in [11] (blue bar) and proposed DET (yellow bar).

TABLE I
PERCENTAGE REDUCTION OF TRIGGERING NUMBER W.R.T. SAMPLED-DATA CONTROLLER IN [29] AND STATIC ET (WITH $\gamma = 0$ IN (22))

| Controller | DG 1 | DG 2 | DG 3 | DG 4 | DG 5 | Total |
|---|---|---|---|---|---|---|
| Sampled Data | −97.18 | −93.8 | −95.7 | −91.89 | −91.87 | −94.1 |
| Static ET | −41.83 | −6.87 | −15.31 | −6.92 | −9.70 | −13.81 |

that static ET triggers more frequently than our DET mechanism. Finally, Table I summarizes the reduction percentage of triggering number ensured by our approach w.r.t. the two alternative controllers. Herein, we can also appreciate that, at the global level, the reduction of the computational burden is of about 94.1% and 13.81%, respectively.

In order to further support our comparison analysis, we also compare the proposed DET control scheme with the following ETC, recently suggested in [11]:

$$\begin{aligned} &u_i = k_U z_i, \quad z_i = \sum_{j\in\mathcal{N}_i}\left(\hat{v}_j - \hat{v}_i\right) + p_i\left(v_{\text{ref}} - \hat{v}_i\right) \\ &t_k = \inf\{t > t_{k-1} | f_i(t) \geq 0, \quad |v_i - v_{\text{ref}}| \geq s \text{ for } p_i = 1 \\ &|z_i| \geq s \text{ for } p_i = 0\} \quad t \in [t_k, t_{k+1}) \end{aligned} \tag{59}$$

with

$$f_i(t) = \left[\hat{v}_i(t) - v_i(t)\right]^2 - \frac{\sigma_i}{4m_i^2}[z_i(t)]^2$$

where $\hat{v}_i(t) = v_i(t_k)$ and $m_i = |\mathcal{N}_i| + 0.5p_i$, being $t_k$ the $k$th trigger time and $|\mathcal{N}_i|$ the cardinality number of the set $\mathcal{N}_i$. According to [11], $k_U = 20,\ s = 2\times10^{-3},\ \sigma_i = 0.9\forall i$, and the overall simulation time is set to 10 [$s$]. The above comparative ETC is actuated at $t = 2$ [$s$] as well. Fig. 9 shows the voltage recovery process performance under the action of the alternative ETC controller (59). Specifically, Fig. 9(c) highlights the total trigger times of comparative controller (59) (blue bar) and our DET strategy (yellow bar). Therefore, by leveraging a dynamic triggering mechanism rather than a static one, the proposed strategy leads to the following significant percentage reductions of the actuator updates: $\approx 90.47\%$, $\approx 70.24\%$, $\approx 76.86\%$, $\approx 63.42\%$, $\approx 65.18\%$ for DG 1, DG 2, DG 3, DG 4 and DG 5, respectively. Besides the highly reduction of the communication burden from controllers-to-actuators achievable via our triggering mechanism, which confirms the superiority of the proposed strategy, it is worth noting that controller (59) only deals with undirected communication topology, thus inherently requiring a greater number of connections among the agents to ensure voltage synchronization, as well as constant voltage reference profile.

## VI. CONCLUSION

This study has introduced a distributed DET PIR control law to solve voltage regulation problem in islanded MG with limited communication network resources. The artificial delay approach, along with LK method, allows proving the exponential voltage recovery in the whole network, while saving network workload via a reduction of sent control inputs number. The derived LMIs stability conditions have allowed finding the upper bounds on sampling period and parameters involved into the DET mechanism preserving voltage stability. Extensive numerical simulations, carried out on the IEEE 14 bus test systems, have confirmed the effectiveness and the robustness of the theoretical derivation. Future works could include the extension of the proposed control scheme with a self-triggered mechanism in order to further reduce both sensing and listening times.

## REFERENCES

[1] M. Yazdanian and A. Mehrizi-Sani, "Distributed control techniques in microgrids," *IEEE Trans. Smart Grid*, vol. 5, no. 6, pp. 2901–2909, Nov. 2014.

[2] T. Qian, Y. Liu, W. Zhang, W. Tang, and M. Shahidehpour, "Event-triggered updating method in centralized and distributed secondary controls for islanded microgrid restoration," *IEEE Trans. Smart Grid*, vol. 11, no. 2, pp. 1387–1395, Mar. 2020.

[3] A. Andreotti, B. Caiazzo, A. Petrillo, and S. Santini, "Distributed robust finite-time secondary control for stand-alone Microgrids with time-varying communication delays," *IEEE Access*, vol. 9, pp. 59548–59563, 2021.

[4] E. Espina, J. Llanos, C. Burgos-Mellado, R. Cardenas-Dobson, M. Martinez-Gomez, and D. Sáez, "Distributed control strategies for microgrids: An overview," *IEEE Access*, vol. 8, pp. 193412–193448, 2020.

[5] B. Ning, Q.-L. Han, and L. Ding, "Distributed finite-time secondary frequency and voltage control for islanded microgrids with communication delays and switching topologies," *IEEE Trans. Cybern.*, vol. 51, no. 8, pp. 3988–3999, Aug. 2021.

[6] M. Keshavarz, A. Doroudi, M. H. Kazemi, and N. M. Dehkordi, "A novel adaptive distributed secondary voltage controller with high convergence rate for islanded microgrids," *IEEE Syst. J.*, vol. 15, no. 3, pp. 4157–4167, Sep. 2021.

[7] S. Zuo, T. Altun, F. L. Lewis, and A. Davoudi, "Distributed resilient secondary control of DC microgrids against unbounded attacks," *IEEE Trans. Smart Grid*, vol. 11, no. 5, pp. 3850–3859, Sep. 2020.

[8] H. Yang, C. Deng, X. Xie, and L. Ding, "Distributed resilient secondary control for AC microgrid under FDI attacks," *IEEE Trans. Circuits Syst. II, Exp. Briefs*, vol. 70, no. 7, pp. 2570–2574, Jul. 2023.

[9] C. Deng, F. Guo, C. Wen, D. Yue, and Y. Wang, "Distributed resilient secondary control for DC microgrids against heterogeneous communication delays and DoS attacks," *IEEE Trans. Ind. Electron.*, vol. 69, no. 11, pp. 11560–11568, Nov. 2021.

[10] G. Zhao, L. Jin, and Y. Wang, "Distributed event-triggered secondary control for islanded microgrids with disturbances: A hybrid systems approach," *IEEE Trans. Power Syst.*, vol. 38, no. 2, pp. 1420–1431, Mar. 2022.

[11] Y. Chen, C. Li, D. Qi, Z. Li, Z. Wang, and J. Zhang, "Distributed event-triggered secondary control for islanded microgrids with proper trigger condition checking period," *IEEE Trans. Smart Grid*, vol. 13, no. 2, pp. 837–848, Mar. 2022.

[12] X. Li, C. K. Ahn, W. Zhang, and P. Shi, "Asynchronous event-triggered-based control for stochastic networked Markovian jump systems with FDI attacks," *IEEE Trans. Syst., Man, Cybern., Syst.*, vol. 53, no. 9, pp. 5955–5967, Sep. 2023.

[13] S. Wang, S. Zheng, C. K. Ahn, P. Shi, and X. Jiang, "Event-triggered cooperative control for uncertain multi-agent systems and applications," *Int. J. Robust Nonlin. Control*, vol. 33, no. 12, pp. 7221–7245, 2023.

[14] P. Ge, B. Chen, and F. Teng, "Event-triggered distributed model predictive control for resilient voltage control of an islanded microgrid," *Int. J. Robust Nonlin. Control*, vol. 31, no. 6, pp. 1979–2000, 2021.

[15] Y. Xie and Z. Lin, "Distributed event-triggered secondary voltage control for microgrids with time delay," *IEEE Trans. Syst., Man, Cybern., Syst.*, vol. 49, no. 8, pp. 1582–1591, Aug. 2019.

[16] B. Zhang, C. Dou, D. Yue, Z. Zhang, and T. Zhang, "A packet loss-dependent event-triggered cyber–physical cooperative control strategy for islanded microgrid," *IEEE Trans. Cybern.*, vol. 51, no. 1, pp. 267–282, Jan. 2021.

[17] A. Girard, "Dynamic triggering mechanisms for event-triggered control," *IEEE Trans. Autom. Control*, vol. 60, no. 7, pp. 1992–1997, Jul. 2015.

[18] Y. Wang, Z. Wang, L. Zou, and H. Dong, "Multiloop decentralized H$\infty$ fuzzy PID-like control for discrete time-delayed fuzzy systems under dynamical event-triggered schemes," *IEEE Trans. Cybern.*, vol. 52, no. 8, pp. 7931–7943, Aug. 2022.

[19] F. Han, X. Lao, J. Li, M. Wang, and H. Dong, "Dynamic event-triggered protocol-based distributed secondary control for islanded microgrids," *Int. J. Elect. Power Energy Syst.*, vol. 137, May 2022, Art. no. 107723.

[20] Y. Li, X. Liu, H. Liu, C. Du, and P. Lu, "Distributed dynamic event-triggered consensus control for multi-agent systems under fixed and switching topologies," *J. Frankl. Inst.*, vol. 358, no. 8, pp. 4348–4372, 2021.

[21] L. Cao, Y. Pan, H. Liang, and T. Huang, "Observer-based dynamic event-triggered control for multiagent systems with time-varying delay," *IEEE Trans. Cybern.*, vol. 53, no. 5, pp. 3376–3387, May 2022.

[22] L. Wen, S. Yu, Y. Zhao, and Y. Yan, "Finite-time dynamic event-triggered consensus of multi-agent systems with disturbances via integral sliding mode," *Int. J. Control*, vol. 96, no. 2, pp. 272–281, 2023.

[23] X. Ge, Q.-L. Han, D. Ding, X.-M. Zhang, and B. Ning, "A survey on recent advances in distributed sampled-data cooperative control of multi-agent systems," *Neurocomputing*, vol. 275, pp. 1684–1701, Jan. 2018.

[24] A. Selivanov and E. Fridman, "An improved time-delay implementation of derivative-dependent feedback," *Automatica*, vol. 98, pp. 269–276, Dec. 2018.

[25] E. Fridman, *Introduction to Time-Delay Systems: Analysis and Control*, (Systems & Control: Foundations & Applications). New York, NY, USA: Springer, 2014.

[26] J. Lai, X. Lu, X. Yu, and A. Monti, "Stochastic distributed secondary control for AC microgrids via event-triggered communication," *IEEE Trans. Smart Grid*, vol. 11, no. 4, pp. 2746–2759, Jul. 2020.

[27] K. Mohammadi, E. Azizi, J. Choi, M.-T. Hamidi-Beheshti, A. Bidram, and S. Bolouki, "Asynchronous periodic distributed event-triggered voltage and frequency control of microgrids," *IEEE Trans. Power Syst.*, vol. 36, no. 5, pp. 4524–4538, Sep. 2021.

[28] Y.-Y. Qian, A. V. Premakumar, Y. Wan, Z. Lin, Y. A. Shamash, and A. Davoudi, "Dynamic event-triggered distributed secondary control of DC microgrids," *IEEE Trans. Power Electron.*, vol. 37, no. 9, pp. 10226–10238, Sep. 2022.

[29] B. Caiazzo, E. Fridman, A. Petrillo, and S. Santini, "Distributed sampled-data PID control for voltage regulation in inverter-based islanded microgrids using artificial delays," *IFAC-PapersOnLine*, vol. 54, no. 18, pp. 186–191, 2021.

[30] G. Lou, W. Gu, J. Wang, W. Sheng, and L. Sun, "Optimal design for distributed secondary voltage control in islanded microgrids: Communication topology and controller," *IEEE Trans. Power Syst.*, vol. 34, no. 2, pp. 968–981, Mar. 2019.

[31] J. Lai, H. Zhou, X. Lu, X. Yu, and W. Hu, "Droop-based distributed cooperative control for microgrids with time-varying delays," *IEEE Trans. Smart Grid*, vol. 7, no. 4, pp. 1775–1789, Jul. 2016.

[32] A. Pilloni, A. Pisano, and E. Usai, "Robust finite-time frequency and voltage restoration of inverter-based microgrids via sliding-mode cooperative control," *IEEE Trans. Ind. Electron.*, vol. 65, no. 1, pp. 907–917, Jan. 2018.

[33] J. Schiffer, R. Ortega, A. Astolfi, J. Raisch, and T. Sezi, "Conditions for stability of droop-controlled inverter-based microgrids," *Automatica*, vol. 50, no. 10, pp. 2457–2469, Oct. 2014.

[34] J. Grainger and W. D. Stevenson, *Power System Analysis*. New York, NY, USA: McGraw-Hill, 1999.

[35] M. S. Hossan, H. M. Maruf, and B. Chowdhury, "Comparison of the ZIP load model and the exponential load model for CVR factor evaluation," in *Proc. IEEE Power Energy Soc. Gener. Meeting*, 2017, pp. 1–5.

[36] A. Selivanov and E. Fridman, "Sampled-data implementation of derivative-dependent control using artificial delays," *IEEE Trans. Autom. Control*, vol. 63, no. 10, pp. 3594–3600, Oct. 2018.

[37] B. Yang et al., "Applications of supercapacitor energy storage systems in microgrid with distributed generators via passive fractional-order sliding-mode control," *Energy*, vol. 187, Nov. 2019, Art. no. 115905.

[38] A. Ramirez, S. Mondie, R. Garrido, and R. Sipahi, "Design of proportional-integral-retarded (PIR) controllers for second-order LTI systems," *IEEE Trans. Autom. Control*, vol. 61, no. 6, pp. 1688–1693, Jun. 2016.

[39] H. K. Khalil, *Nonlinear Systems Third Edition*. Upper Saddle River, NJ, USA: Prentice Hall, 2002.

[40] E. Fridman and L. Shaikhet, "Delay-induced stability of vector second-order systems via simple Lyapunov functionals," *Automatica*, vol. 74, pp. 288–296, Dec. 2016.

[41] E. Fridman and L. Shaikhet, "Stabilization by using artificial delays: An LMI approach," *Automatica*, vol. 81, pp. 429–437, Jul. 2017.

[42] A. Selivanov and E. Fridman, "Simple conditions for sampled-data stabilization by using artificial delay," *IFAC-PapersOnLine*, vol. 50, no. 1, pp. 13295–13299, 2017.

[43] X. Ge, Q.-L. Han, L. Ding, Y.-L. Wang, and X.-M. Zhang, "Dynamic event-triggered distributed coordination control and its applications: A survey of trends and techniques," *IEEE Trans. Syst., Man, Cybern., Syst.*, vol. 50, no. 9, pp. 3112–3125, Sep. 2020.

[44] A. Selivanov and E. Fridman, "Robust sampled-data implementation of PID controller," in *Proc. IEEE Conf. Decis. Control (CDC)*, 2018, pp. 932–936.

[45] C. Huang, G. Zhai, and G. Xu, "Necessary and sufficient conditions for consensus in third order multi-agent systems," *IEEE/CAA J. Automatica Sinica*, vol. 5, no. 6, pp. 1044–1053, Nov. 2018.

[46] X. Yi, K. Liu, D. V. Dimarogonas, and K. H. Johansson, "Dynamic event-triggered and self-triggered control for multi-agent systems," *IEEE Trans. Autom. Control*, vol. 64, no. 8, pp. 3300–3307, Aug. 2019.

[47] D. V. Dimarogonas, E. Frazzoli, and K. H. Johansson, "Distributed event-triggered control for multi-agent systems," *IEEE Trans. Automat. control*, vol. 57, no. 5, pp. 1291–1297, May 2012.

[48] *IEEE Guide for Design, Operation, and Integration of Distributed Resource Island Systems with Electric Power Systems*, IEEE Standard 1547.4-2011, Jul. 2011.

[49] D. Ghaderyan, F. L. Pereira, and A. P. Aguiar, "A fully distributed method for distributed multiagent system in a microgrid," *Energy Reports*, vol. 7, pp. 2294–2301, Nov. 2021.

[50] A. Kumar, B. K. Jha, S. Das, and R. Mallipeddi, "Power flow analysis of islanded microgrids: A differential evolution approach," *IEEE Access*, vol. 9, pp. 61721–61738, 2021.

[51] A. Andreotti, B. Caiazzo, A. Petrillo, S. Santini, and A. Vaccaro, "Robust finite-time voltage restoration in inverter-based microgrids via distributed cooperative control in presence of communication time-varying delays," in *Proc. IEEE Int. Conf. Environ. Elect. Eng. Proc. IEEE Ind. Commer. Power Syst. Europe (EEEIC/I CPS)*, 2020, pp. 1–6.

[52] F. Guo, C. Wen, J. Mao, and Y.-D. Song, "Distributed secondary voltage and frequency restoration control of droop-controlled inverter-based microgrids," *IEEE Trans. Ind. Electron.*, vol. 62, no. 7, pp. 4355–4364, Jul. 2015.

[53] V. Nasirian, Q. Shafiee, J. M. Guerrero, F. L. Lewis, and A. Davoudi, "Droop-free distributed control for AC microgrids," *IEEE Trans. Power Electron.*, vol. 31, no. 2, pp. 1600–1617, Feb. 2016.


Open Access funding provided by 'Università degli Studi di Napoli "Federico II"' within the CRUI CARE Agreement